1-1-2019

The Archean Victoria Fjord terrane of northernmost Greenland and geodynamic interpretation of Precambrian crust in and surrounding the Arctic Ocean

Allen Phillip Nutman
University of Wollongong, anutman@uow.edu.au

Vickie C. Bennett
Australian National University (ANU), vickie.bennett@anu.edu.au

Hiroshi Hidaka
Nagoya University, University of Hiroshima

Niels Henriksen
Geological Survey of Denmark and Greenland

Sarmad A. Ali
University of Wollongong, sarmad@uow.edu.au

The Archean Victoria Fjord terrane of northernmost Greenland and geodynamic interpretation of Precambrian crust in and surrounding the Arctic Ocean

Abstract

In far North Greenland at the head of Victoria Fjord (~81°30'N), a ~1000 km 2 exposure of Precambrian crystalline basement rocks is a window through the region's extensive latest Neoproterozoic and Paleozoic Arctic Platform sedimentary cover sequence. These basement rocks, named here the Victoria Fjord terrane, are dominated by weakly-foliated granodioritic orthogneisses, with lesser amounts of migmatite. These are intercalated with strips of supracrustal rocks dominated by paragneisses. This poorly-exposed Archean terrane at Greenland's northern tip is succeeded to the south by the extensive east-west trending Paleoproterozoic Inglefield Mobile Belt of juvenile arc rocks. The Victoria Fjord terrane granodiorites have zircon U-Pb ages from 3292 ± 14 Ma to ~3260 Ma. Reconnaissance U-Pb dating on schlieric migmatite zircons yielded ages of ~3280, 3400 and 3500 Ma. Paragneiss detrital zircons have ages of mostly ~2710 Ma, with a minority of 3000-2900 Ma grains. This demonstrates that these sedimentary rocks were not derived from the local basement. Post- Archean magmatic or metamorphic zircon was not detected in any of the samples. Initial ε Hf of 3290-3260 Ma granodiorite and granite zircons ranges from −4 to +2, and the magmatic protoliths are interpreted as sourced from the melting of somewhat older (3500-3400 Ma) Paleoarchean crust, represented by paleosome in the migmatites. The paragneiss 3000-2900 Ma detrital zircons were derived from juvenile felsic crust of that age. The ~2710 Ma group show negative correlation of Th/U and initial ε Hf , such that those with high Th/U up to >2.0 have ε Hf values of −6 to −10. The ~2710 zircons were sourced from mafic rocks formed by melting of much older (Paleoarchean?) enriched mantle which was variably contaminated by 3000-2900 Ma crust during its ascent. The Victoria terrane is unique amongst the Archean basement terranes in Greenland because it is dominated by 3500-3260 Ma crust. However, the Arctic basin contains detrital zircons of that age, and rocks of that age also occur in eastern Siberia and northwestern Canada. Implications for high Arctic early Precambrian geodynamics are discussed.

Publication Details

Nutman, A. P., Bennett, V. C., Hidaka, H., Henriksen, N. & Ali, S. (2019). The Archean Victoria Fjord terrane of northernmost Greenland and geodynamic interpretation of Precambrian crust in and surrounding the Arctic Ocean. Journal of Geodynamics, 129 3-23.

The Archean Victoria Fjord terrane of northernmost Greenland and geodynamic interpretation of Precambrian crust in and surrounding the Arctic Ocean

Published in: Journal of Geodynamics (2019), 129 3-23

Allen P. Nutman[1], Vickie C. Bennett[2], Hiroshi Hidaka[3,4], Niels Henriksen[5] and Sarmad Ali[1,6]

1 GeoQuEST Research Centre, School of Earth, Atmospheric and Life Sciences, University of Wollongong, Wollongong, NSW 2522, Australia

2 Research School of Earth Sciences, The Australian National University, Canberra, ACT 0200, Australia

3 Department of Earth Systems Sciences, Hiroshima University, Higashi Hiroshima, 739-8511, Japan

4 Department of Earth and Planetary Sciences, Nagoya University, Nagoya, 464-8601, Japan

5 Geological Survey of Denmark and Greenland, Øster Voldgade 10, 1350 Copenhagen K, Denmark

6 Department of Applied Geology, College of Science, Kirkuk University, Kirkuk 36001, Iraq

Email contact: anutman@uow.edu.au

Abstract:

In far North Greenland at the head of Victoria Fjord (~81°30'N), a ~1000 km^2 exposure of Precambrian crystalline basement rocks is a window through the region's extensive latest Neoproterozoic and Paleozoic Arctic Platform sedimentary cover sequence. These basement rocks, named here the *Victoria Fjord terrane*, are dominated by weakly-foliated granodioritic orthogneisses, with lesser amounts of migmatite. These are intercalated with strips of supracrustal rocks dominated by paragneisses. This poorly-exposed Archean terrane at Greenland's northern tip is succeeded to the south by the extensive east-west trending Paleoproterozoic Inglefield Mobile Belt of juvenile arc rocks.

The Victoria Fjord terrane granodiorites have zircon U-Pb ages from 3292 ± 14 Ma to ~3260 Ma. Reconnaissance U-Pb dating on schlieric migmatite zircons yielded ages of ~3280, 3400 and 3500 Ma. Paragneiss detrital zircons have ages of mostly ~2710 Ma, with a minority of 3000-2900 Ma grains. This demonstrates that these sedimentary rocks were *not* derived from the local basement. Post-Archean magmatic or metamorphic zircon was not detected in any of the samples.

Initial ε_{Hf} of 3290-3260 Ma granodiorite and granite zircons ranges from -4 to +2, and the magmatic protoliths are interpreted as sourced from the melting of somewhat older (3500-3400 Ma) Paleoarchean crust, represented by paleosome in the migmatites. The paragneiss 3000-2900 Ma detrital zircons were derived from juvenile felsic crust of that age. The ~2710 Ma group show negative correlation of Th/U and initial ε_{Hf}, such

that those with high Th/U up to >2.0 have ε_{Hf} values of -6 to -10. The ~2710 zircons were sourced from mafic rocks formed by melting of much older (Paleoarchean?) enriched mantle which was variably contaminated by 3000-2900 Ma crust during its ascent.

The Victoria terrane is unique amongst the Archean basement terranes in Greenland because it is dominated by 3500-3260 Ma crust. However, the Arctic basin contains detrital zircons of that age, and rocks of that age also occur in eastern Siberia and northwestern Canada. Implications for high Arctic early Precambrian geodynamics are discussed.

Keywords: North Greenland; Arctic Ocean; Victoria Fjord terrane; Paleoarchean

1. Introduction

The reconstruction of Precambrian crustal evolution in the northern polar region is less advanced than in many other parts of the globe, because of its remoteness adding greatly to the expense and difficulty of geological field expeditions. For the extended ribbons of continental crust within the expanding Arctic Ocean (e.g., Grantz et al., 1990, 2011; Pease et al., 2014; Pease and Coakley, 2018), the difficulties are hampered even further by sea ice, which precludes conventional ship-based sampling of the sea floor. Finally, around the Arctic Ocean, the Precambrian basement is largely obscured by latest Neoproterozoic to Phanerozoic sedimentary platform sequences, meaning that basement provinces and lineaments cannot be followed with confidence over long distances.

This paper contributes to understanding the Archean and Paleoproterozoic evolution of the northern polar region by (i) reporting the first integrated geochemical and zircon U-Pb-Hf data from the Archean basement terrane at the head of Victoria Fjord in far North Greenland (Fig. 1) and (ii) integrating this with published information from the rest of Greenland, the Arctic Ocean and early Precambrian terranes in eastern Siberia. We stress that this paper has the purpose of neither contributing to detailed understanding of the Cretaceous and Cenozoic stages of Arctic Ocean opening (e.g., Grantz et al., 2011; Pease and Coakley, 2018) nor for the purpose of entering into debates concerning the evolution and disposition of early Precambrian continents such as Vaalbara and Ur (e.g., Rogers, 1996; Zegers et al., 1998; Nance et al., 2014). Instead, the purpose is to highlight the similarity of the

79 North Greenland Victoria Fjord terrane's early Archean ages with detritus in the Arctic
80 Ocean (e.g., Presnyakov et al., 2014) and basement massifs in eastern Siberia (e.g.,
81 Bibikova et al., 1988, 2006; Nutman et al., 1992;), and then stress the contrast with
82 the age components from all Archean terranes farther south in the rest of Greenland.
83 The early Precambrian geodynamic significance of this is explored via a Phanerozoic
84 analogue; the life cycle of the Neotethys Ocean between Gondwana and Eurasia.
85
86 **2. Geology of North Greenland and the Victoria Fjord terrane**
87 *2.1. Regional crustal evolution*
88 Early Precambrian Greenland consists of a collage of approximately east-west
89 trending Paleoproterozoic mobile belts interspersed with blocks of Archean basement
90 rocks showing variable degrees of reworking in Paleoproterozoic orogenies (Fig. 1
91 inset; e.g., Kalsbeek, 1981, 1986; Nutman et al., 2008a). The Paleoproterozoic mobile
92 belts contain convergent plate boundary and magmatic arc sequences (e.g., Kalsbeek
93 et al., 1987; Kalsbeek and Nutman, 1996; Nutman et al., 1999, 2008a,b; Whitehouse
94 et al., 1998; Connelly et al., 2000; Garde et al., 2002). The extinction of these arcs
95 was caused by consumption of Paleoproterozoic ocean(s) and the collision with
96 Archean continental crust on either side (Kalsbeek et al., 1987, Kalsbeek and Nutman,
97 1996; Nutman et al., 2008b). Thus, the Paleoproterozoic mobile belts are suture zones,
98 in which the arc assemblages have been dismembered by late tectonic movements,
99 and in which Paleoproterozoic relict high pressure metamorphic assemblages up to
100 eclogite facies record crustal thickening during collisional orogeny (e.g., Nutman et

al., 2008b; Müller et al., 2018). The northern-most of these mobile belts is the Inglefield Mobile Belt, which traverses Greenland east-west, to the south of the Victoria Fjord terrane (Fig. 1 inset; Dawes, 2009; Nutman et al., 2008a). This belt might continue into North East Greenland (Nutman et al., 2008b), but there is uncertainty due to the allochthonous nature of the Precambrian basement inliers of the Caledonian orogen (e.g., Kalsbeek et al., 1993).

Crystalline basement in northernmost Greenland is overlain by homoclinal sequences of the Arctic platform (Trettin, 1991). These sequences are prominent, hampering the regional correlation of crystalline basement units. At the heads of some fjords, such as the Victoria Fjord focused on in this paper, erosion has cut through the Arctic platform sequences, and rocks of the shield are exposed in nunataks (Fig. 1). The most extensive basement exposures are to the south and west of Victoria Fjord on Inglefield Land and northern Prudhoe Land, where they are dominated by the Paleoproterozoic Inglefield Mobile Belt (Fig. 1 inset; Schjøth et al., 1996; Steenfelt and Dam, 1996; Thomassen and Dawes, 1996; Dawes et al., 2000; Thomassen et al., 2002; Nutman et al., 2008a). The belt is dominated by juvenile 2000-1950 Ma plutonic and sedimentary rocks of arc-like geochemical affinity, in tectonic contact on the southern side with an early Paleoproterozoic clastic sedimentary and carbonate sequence and Archean basement (Dawes and Frisch, 1981; Nutman, 1984; Dawes et al., 1988; Thomassen et al., 2002; Dawes, 2006; Nutman et al., 2008a).

123 *2.2. Victoria Fjord terrane*

124 From aerial photographs, nunataks on the northern fringe of the Inland Ice at the
125 head of Victoria Fjord (Fig. 1) were noted as 'anomalous' in appearance compared
126 with neighbouring nunataks, and on early maps were shown as basement to the
127 extensive Arctic platform sequence (Haller, 1961; GGU, 1970). We name here these
128 basement rocks as the *Victoria Fjord terrane*. The first ground-based studies found
129 these nunataks to consist of granitic gneisses and amphibolites (Dawes, 1976, 1978;
130 Hurst and Peel, 1979). A reconnaissance geological map was produced in 1984
131 (Henriksen and Jepsen, 1985) as part of a broader project to compile a regional
132 1:500,000 scale geological map of entire northeastern Greenland. Because of the
133 remoteness of this area, needing large state-sponsored expeditions to undertake
134 scientific work, the Victoria fjord basement terrane has not been visited for over 30
135 years, and the preliminary map, geological interpretation and associated sampling by
136 Henriksen and Jepsen (1985) is the most detailed appraisal of the geology. It is for this
137 reason that only a broad description of the field geology can be presented here.

138 The Victoria Fjord terrane is exposed over ~1000 km^2 in lower reaches of valleys
139 and on six nunataks at the head of Victoria Fjord (Fig. 1). Apart from the remoteness
140 of the area limiting geological study to several decades ago, another issue with the
141 Victoria Fjord terrane is that its upper surface is a late Neoproterozoic erosional and
142 weathering surface. Given that the terrane is dominated by evolved granitic rocks with
143 mostly high-U zircons, ancient radiogenic Pb loss giving discordant ages is common
144 in our zircon data. This means that in some cases the rock ages are imprecise, due to

145 the complex 2 or 3 stage history of the zircons. From the 1980s reconnaissance study
146 when, for time and logistical constraints, nonetheless it was not possible to visit all
147 outcrops, it appears that there are no major lithological differences across the exposed
148 terrane. Henriksen and Jepsen (1985) describe the dominant lithology to be pale
149 weathering, homogeneous leucocratic orthogneisses, with variations both to foliated
150 granites and, with increased leucosome fractions, into migmatitic rocks. The
151 orthogneisses are cut by subconcordant veins and sharply cross-cutting bodies of
152 pegmatite. Thin supracrustal packages of dominantly metasedimentary origin are
153 interleaved as concordant strips within the gneisses. There is insufficient field
154 evidence to indicate whether the orthogneisses or the metasedimentary rocks are the
155 oldest. The metasedimentary units consist of mica schists, marble, siliceous schists,
156 quartzites and amphibolite, and commonly carry garnet. Sharp-bordered amphibolite
157 sheets are common, and these can reach 30 m thick (Henriksen and Jepsen, 1985).
158 These are locally discordant to the foliation in their country rocks and represent
159 deformed and metamorphosed mafic dykes.
160 Conventional ID-TIMS U–Pb multigrain zircon analyses (2 samples) and K–Ar
161 analyses on hornblende were carried out on Victoria Fjord terrane rocks (Hansen et al.,
162 1987). The zircon samples contained considerable common Pb and yielded strongly
163 discordant results, but nonetheless indicated that the examined rocks are Archean in
164 age. Amphibole K–Ar analyses gave ages of ~1850 Ma that were interpreted to reflect
165 closure to Ar diffusion after a Paleoproterozoic thermal event (Hansen et al., 1987).
166 Results of SHRIMP U-Pb zircon dating on one granitic gneiss (sample GGU312632,

167 previously studied with the bulk zircon ID-TIMS method by Hansen et al., 1987)
168 indicated a Paleoarchean age, with magmatic zircon of 3401±12 Ma and with
169 recrystallisation in a thermal event at ~3280 Ma (Nutman et al., 2008a). Ages from
170 sample GGU312632 are integrated with the new results presented in this paper.
171
172 **4. Analytical methods**
173 *4.1. Major and trace element geochemistry*
174 Samples were crushed using a Cr-Ni TEMA ring grinder. Fused buttons were made
175 for X–ray fluorescence (XRF) major element analysis. The samples were oxidised by
176 adding 5 ml of lithium nitrate solution and left at 60°C overnight, before being fused
177 in a furnace. Pressed pellets for XRF trace element analysis were created by mixing ~
178 5 g of sample with a polyvinyl acetate (PVA) binder and pressed into an aluminum
179 cup using a hydraulic hand press. The pressed pellets were then oven dried at 60°C for
180 4 hours. Major and a suite of trace element analysis (Table 1) were conducted using a
181 SPECTRO XEPOS X–ray fluorescence spectrometer at the University of Wollongong,
182 following the methods of Norrish and Chappell (1977). W-2 dolerite standard (n = 4),
183 which was used during the period that data for this paper were acquired, shows a
184 standard deviation < 3% for all the major elements and agrees with accepted values.
185 Rare earth elements (REE) and an additional suite of trace elements (Table 1) were
186 analysed by ALS Minerals Division Brisbane via ICP–MS, (geochemical procedure
187 ME-MS81). A prepared sample is added to lithium metaborate/lithium tetraborate flux,
188 mixed well and fused in a furnace. The resulting melt is then cooled and dissolved in

189 an acid mixture containing nitric, hydrochloric and hydrofluoric acids. This solution is
190 then analysed by ICP–MS. Standards, OREAS 120 and STSD-1, were duplicated for
191 the run as well as 5 sample duplicates and 3 blanks, with a <10% tolerance of error
192
193 *4.2. SHRIMP U-Pb zircon geochronology*
194 Zircons were concentrated from crushed rock powder using heavy liquid and
195 isodynamic separation techniques at the mineral separation laboratory of the Research
196 School of Earth Sciences, the Australian National University (ANU). Using a
197 binocular microscope, the concentrate was hand-picked and along with reference
198 Temora-2 zircons (Black et al., 2003), the selected grains were cast in an epoxy resin
199 disc. The disc was ground to reveal a mid-section level through the grains and then
200 polished. Cathodoluminescence (CL) imaging was used to document the grains.
201 U-Th-Pb analyses of the zircons were undertaken on the Hiroshima University
202 SHRIMP 2 instrument following analytical protocols of Williams (1998), with the raw
203 data being reduced using ANU software 'PRAWN' and 'LEAD'. These older software
204 were preferred to more recent packages, due to the higher efficacy of PRAWN in
205 assessing disturbed zircons, where particularly submicron-scale movement of lead has
206 resulted in much noise in ^{206}Pb and ^{207}Pb data, requiring special attention to ensure
207 authentic, full error propagation. Measurements of $^{206}Pb/^{238}U$ in unknown zircons
208 were calibrated using the Temora-2 standard (U-Pb ages concordant at 417 Ma; Black
209 et al., 2003). The reference zircon SL13 (U=238 ppm) located in a set-up mount was
210 used to calibrate U and Th abundance in the unknown zircons. Correction for

common Pb was based on measured ^{204}Pb and the Cumming and Richards (1975) late Neoproterozoic Pb composition. This composition was chosen because the trend of discordant data arrays trend to a lower concordia intercept at this time – linked to erosion and weathering.

The ISOPLOT-3 program (Ludwig, 2003) was used to assess and plot the reduced and calibrated data. Regression in $^{207}Pb/^{206}Pb$ – $^{238}U/^{206}Pb$ space and $^{207}Pb/^{206}Pb$ ratios for close to concordant analyses were used to calculate ages. In the former, the upper intercept with concordia is interpreted as the radiogenic (i.e. magmatic) dominant component, whereas the lower intercept signifies the time of disturbance. The U-Pb data sets frequently show evidence of more than one episode of ancient Pb loss. One is definitely in the late Neoproterozoic – early Paleozoic, probably due to proximity to a weathered surface. Some data suggest another event perhaps in the Paleoproterozoic, related to zircon recrystallisation during a tectonothermal disturbance at that time. Finally, for >3300 Ma oldest zircons, another event probably occurred in the late Paleoarchean, at the time of the significant ~3300 Ma magmatic event. For this reason, discordant data, if all regressed together, will tend to have a MSWD>1, i.e. the U-Pb systematics cannot be accounted for by simply concordia intercepts indicating T1 when the zircons formed and T2 the time of only a single episode of radiogenic Pb loss. Where more than one episode of radiogenic Pb loss is revealed in the data, analyses plotting close to the concordia upper intercept, but with apparently young ages, were rejected in the regression process. The rationale is that one is removing the oldest episode of Pb disturbance, and thereby the increased age of the upper concordia

intercept will give a better estimate of the time of magmatic zircon crystallisation. All calculated ages are presented at 95% confidence and are rounded to the nearest million years.

4.3. LA-ICP-MS Lu-Hf isotopic data

Zircon Lu-Hf isotopic compositions were determined from the same domains as the U-Pb geochronology, as determined by CL imagery. Most of these were positioned directly over the previous SHRIMP U-Pb analysis 1-2 micron-deep craters, with a minority of other analyses undertaken on other domains with relict oscillatory zoning displayed in CL images. Data were acquired during a single analytical session using the RSES ThermoFinnigan Neptune multi-collector ICPMS coupled to a Lambda Physik ArF, 193 nm excimer laser system with a 'HelEx' sample cell, following methods described by Hiess et al. (2009) and using a 42 μm diameter spot. Analysis of a gas blank and a suite of 6 reference zircons with a range of $^{176}Hf/^{177}Hf$ and $^{176}Lu/^{177}Hf$ ratios (Monastery, Mud Tank, Plesovice, QGNG, R33 and FC1) were performed systematically after every 10-12 sample spot analyses throughout the session. The details of the analytical method and instrumental set-up are provided in the Supplementary Data. The $^{176}Hf/^{177}Hf$ isotopic compositions determined for the reference zircons are in all cases within error (better than 0.5 epsilon units) of accepted values.

Complete Lu-Hf isotopic data for the sample zircons and for zircons for the 6 reference materials including $^{174}Hf/^{177}Hf$ and $^{178}Hf/^{177}Hf$ isotopic compositions are

given in Supplementary Data Tables 1 and 2.

Initial $^{176}Hf/^{177}Hf$ ratios for each spot were calculated using SHRIMP measured U-Pb ages, present day CHUR compositions of $^{176}Hf/^{177}Hf = 0.282785\pm11$, $^{176}Lu/^{177}Hf = 0.0336\pm1$ (Bouvier et al. 2008), and a $\lambda^{176}Lu$ decay constant of $1.867\pm8 \times 10^{-11} y^{-1}$ (Scherer et al. 2001; Söderlund et al. 2004).

5. Petrography and whole rock geochemistry

5.1. Petrography

The predominant rock type is granodioritic and medium-grained (Table 1, sample GGU312611 on supplementary Fig. 1A). Most samples are homogeneous and weakly foliated with a granoblastic texture (GGU312610, -611, -31, -96), whereas others (GGU312630 this paper and -632 in Nutman et al., 2008a) are migmatitic. They contain quartz + K-feldspar + plagioclase+ biotite ± secondary muscovite ± hornblende + iron oxides + trace zircon and apatite. All samples show breakdown of plagioclase to albite + fine-grained dusting of white mica + epidote. This alteration is least in sample GGU312696 (supplementary Fig. 1B), which also yielded the most concordant U-Pb zircon ages. All samples contain biotite, but the migmatite sample GGU312630 (supplementary Fig. 1C) contains hornblende in its likely paleosome component.

Two metasedimentary samples examined were quartzite GGU312658 and mica schist -653 (Table 1). Quartzite GGU312658 contains abundant quartz, together with K-feldspar + muscovite + biotite + plagioclase, with the two micas defining a foliation.

On the scale of the small hand specimen (<1 kg) it is homogeneous and devoid of relict sedimentary structure. Mica schist GGU312653 (supplementary Fig. 1D) consists of <2 mm garnet porphyroblasts + biotite + quartz + plagioclase. The biotite is partly chloritised and defines a foliation. Both the metasedimentary samples have traces of zircon and apatite. Both the orthogneisses and paragneisses display a single foliation, which in most samples is weak. This suggests superimposition on the entire complex of only weak ductile deformation.

5.2. Whole rock geochemistry

Whole rock analyses of the samples upon which U-Pb zircon dating was undertaken are presented in Table 1. The (meta)granitoids all have similar SiO_2 contents of ~71 wt%, with high total $Na_2O + K_2O$. The composite analysis of migmatite sample GGU312630 is similar to the homogeneous samples (Table 1). On the Zr/Ti – SiO_2 discrimination diagram, all these samples fall in the field of granodiorite (Fig. 2a). In a chondrite-normalised REE plot (Fig. 3a) all the granitic rocks display enrichment of the light relative to the heavy REE with slightly downward-bowed patterns, but with all elements enriched relative to chondrite. There are no significant Eu anomalies, indicating that igneous fractionation of plagioclase was not a significant factor in their petrogenesis. In the primitive mantle normalised trace element (spider) diagram (Fig. 3c) all granitoid samples show enrichment in the large ion lithophile elements, with notable negative anomalies of the high field strength elements Nb, Ta and Ti. These patterns are typical for granitoids in the

299 continental crust. An anomalous feature in the patterns is that several samples show
300 distinct negative Sr anomalies, without 'supporting' negative Eu anomalies which
301 would be indicative of magmatic plagioclase fractionation. One possibility is that this
302 is a secondary feature that originated from anorthite breakdown with Sr release during
303 late Neoproterozoic weathering. Support for this interpretation comes from sample
304 GGU312696, which in thin section indicates the plagioclase is the least altered of all
305 the samples, and yet it displays no negative Sr anomaly (Fig. 3c) and that its zircons
306 are the least metamict. On a Y+Nb – Rb discrimination diagram the granitoid samples
307 fall within the upper part of the volcanic arc granite (VAG) field (Fig. 2B).
308 The two metasedimentary samples GGU312653 and -658 have markedly different
309 whole rock compositions. Impure quartzite sample GGU312658 is dominated by
310 quartz and muscovite, and minor biotite and K-feldspar. It has low content of
311 ferromagnesian elements, but with Al_2O_3 and K_2O being the second-most abundant
312 components after SiO_2 (Table 1). The schist sample GGU312653 has lower SiO_2 and
313 higher ferromagnesian element abundances. In both samples, Na_2O/K_2O is low,
314 indicative of highly weathered source materials, rather than an immature arkosic
315 component being present. In a PAAS-normalised (Post Archean Average Shale) REE
316 plot, both samples display sub-PAAS values. The schist sample GGU312653 displays
317 heavy REE enrichment relative to the light REE (Fig. 3B) and high Ni+Cr, whereas
318 the quartzite sample GGU312658 has slight enrichment of the light REE over the
319 heavy REE (Fig. 3B). The difference in the REE patterns between the samples
320 indicates that in the protolith sedimentary rocks there is not simply a single

REE-bearing detrital component variably diluted by detrital quartz (a mineral essentially devoid of REE). Instead it is likely that the REE signatures of these rocks reflect two discrete sources, the one in the schist being predominantly a ferromagnesian high Ni+Cr source, such as weathered mafic/intermediate rocks, whereas the quartzite shows stronger input from a weathered felsic source.

6. U-Pb-Hf zircon data

6.1. U-Pb zircon

Foliated granodioritic sample GGU312610 (SiO_2 = 71.96 and K_2O = 4.10 wt%) contains prismatic zircons up to ~200 μm long. They are overall dull in CL images, with only parts of them displaying relict oscillatory zoning of igneous origin (Fig. 4). All grains seem to be single component, without inherited cores or overgrowths. U-Pb analyses focused on domains that appear less dull in CL images, and therefore less likely to have been modified by metamictisation. None the less, U and Th abundances in these sites are high (up to 1795 and 340 ppm respectively; Table 2). Common Pb content is low, with the U-Pb analyses forming a discordant array, with four analyses yielding concordant within error ages (Fig. 5a). Regression of all the data gives upper and lower concordia intercepts of 3280 ± 30 and 870 ± 400 Ma respectively, whereas the two closest to concordant analyses yield a weighted mean $^{207}Pb/^{206}Pb$ age of 3288 ± 14 Ma (MSWD=0.62). The latter is taken as the most likely igneous protolith age of granitic sample GGU312610.

Foliated granodioritic sample GGU312611 (SiO_2 = 71.60 and K_2O = 1.44 wt%)

343 contains prismatic zircons up to ~200 μm long. They are overall less dull in CL
344 images than the sample GGU312610 grains, so that more of their internal structure is
345 visible. The grains are strongly recrystallised with only vestiges of igneous-style
346 oscillatory zoning surviving. U abundances are high (mostly >1000 ppm), but Th
347 abundances are generally lower, giving rise to Th/U ratios from 0.07 to 0.51 (Table 2).
348 This probably reflects the pervasive recrystallisation of these zircons. All analyses
349 yield discordant U-Pb ages, and scatter well beyond a single Pb-loss trajectory (Fig.
350 5b). The $^{207}Pb/^{206}Pb$ age of 3260 Ma for analysis 4.2 (concordance 70%) is interpreted
351 as giving the minimum magmatic age for granodiorite sample GGU312611.
352 Foliated granodiorite sample GGU312631 (SiO_2 = 71.71 and K_2O = 2.70 wt%)
353 yielded zircons similar in size, morphology and CL characteristic as GGU312611, but
354 with somewhat greater preservation of oscillatory igneous zoning with analysis 6.1
355 being a possible inherited core. U contents range from 92 to 755 ppm and Th/U from
356 0.002 to 0.67, with the former probably reflecting the variable degrees of post
357 magmatic recrystallisation seen in the CL imagery. Common Pb content is low, apart
358 from in the most discordant analysis 8.1. The U-Pb analyses form a discordant array
359 (Fig. 5c), with variably discordant U-Pb ages, and upper and lower intercepts of 3349
360 ± 190 and 1545 ± 480 Ma, respectively, but with scatter well beyond a single Pb-loss
361 trajectory (MSWD=18). Possible core analysis 6.1 is concordant within analytical
362 error, with the oldest $^{207}Pb/^{206}Pb$ age of 3353 ± 16 Ma (2 σ). Rejecting analysis 4.1
363 with a younger age, the remaining concordant and close to concordant analyses yield
364 a weighted mean $^{207}Pb/^{206}Pb$ age of 3256 ± 24 Ma (MSWD=1.08). The data are

365 interpreted to indicate a protolith age of ~3260 Ma, probably with older inherited
366 components present.

367 Foliated granodiorite sample GGU312696 (SiO_2 = 72.29 and K_2O = 2.52 wt%)
368 yielded prismatic zircons up to 200 µm long, which in CL images show widespread
369 preservation of oscillatory igneous zonation, overprinted by variable degrees of
370 patchy recrystallisation (Fig. 4). Uranium contents range from 145 to 938 ppm with
371 Th/U between 0.12 and 0.94 (Table 2). Most analyses are concordant and close to
372 concordant apart from site 2.1 (Fig. 5d), which also has the highest U content.
373 Excluding two discordant data, the remaining 6 analyses yield a weighted
374 mean $^{207}Pb/^{206}Pb$ age of 3294 ± 14 Ma (MSWD=0.59), which is interpreted as the
375 igneous protolith age of granodiorite sample GGU312610. The overall lower U
376 content of the zircons and the overall greater freshness of this sample compared with
377 other Victoria metagranitoids are the reasons for the more concordant data.

378 Banded gneiss/migmatite sample GGU312630 (with average SiO_2 = 72.73 and
379 K_2O = 3.51 wt%) yielded mostly prismatic zircon up to ~150 µm long. In CL images
380 they appear overall dull, but with complex recrystallisation textures dominating the
381 grains, greatly limiting the choice of sites for analysis (Fig. 4), and only five U-Pb
382 analyses were undertaken. Three of these (2.1, 3.1 and 4.1) yield close to concordant
383 ages, but with a spread in apparent $^{207}Pb/^{206}Pb$ ages from ~3516 to ~3270 Ma (Table 2,
384 Fig. 5e). These analyses display low U abundances of <400 ppm, whereas the two
385 analyses with highly discordant U-Pb ages have much higher U abundance to >2000
386 ppm (Table 2). The spread of $^{207}Pb/^{206}Pb$ ages for the most concordant sites could be

interpreted as; (i) indicating solely ~3500 Ma zircon is present, which suffered Pb loss in a thermal event at ~3300 Ma, when granitic rocks were emplaced, or (ii) that the rock has two components ~3500 and ~3300 Ma. Given the heterogeneous migmatitic character of the rock, the latter interpretation from this reconnaissance dataset is preferred.

Banded gneiss /migmatite sample GGU312632 was reported in Nutman et al. (2008a) and the results are summarized here (Fig. 5f and Table 2). The zircons in this sample, like other metagranitoids from Victoria Fjord, are markedly affected by post-magmatic recrystallisation. In sample GGU312632 a protolith magmatic age of 3401 ± 12 Ma, an early recrystallisation event at ~3280 Ma followed by Neoproterozoic to Paleozoic Pb loss was proposed.

Mica schist sample GGU312653 and siliceous schist sample GGU312658 both yielded abundant zircons that are mostly 100-150 μm long. The zircon morphology in both samples is mostly ovoid to rounded-prismatic. They widely preserve oscillatory zoning, but in many grains this is truncated at the grain exterior or is mantled by a narrow (<5 μm) recrystallisation fringe that is bright and featureless in CL images (Fig. 4). The grains are interpreted as detrital in origin, affected by minor recrystallisation.

In each of samples GGU312653 and GGU312658, 20 analyses were undertaken on 20 zircons (Table 2). Only the oscillatory-zoned zircon was analysed, because all the bright homogeneous rims are too narrow to accommodate a 15-20 μm analytical spot. All sites have moderate U content (mostly <500 ppm) and high Th/U, which,

409 combined with the oscillatory zoning of the sites, indicates the grains are derived from
410 igneous sources. The low U content of the zircons is the likely reason for the limited
411 loss of radiogenic Pb, compared with the zircons in the Paleoarchean metagranitoids
412 and gneisses. Most of the sites yielded U-Pb ages that are concordant, with both
413 samples showing the same age distribution (Table 2; Fig. 6). Most grains (>30) have
414 an age of ~2710 Ma with the remainder having ages of ~2900-3000 Ma. The slight
415 skewness of the 2715 population is caused by minor ancient Pb loss with discordancy
416 in a few analyses. Most notable is that none of these detrital grains match in age the
417 3300-3500 Ma components in the adjacent metagranitoids, suggesting a distal source.
418 Also notable is the overall very high Th/U of typically >1.0 for the ~2710 Ma grains.
419 The significance of this is explored below.
420
421 *6.2. Lu-Hf in zircon*
422 One hundred and two zircon Lu-Hf analyses were undertaken (Table 3). For sites
423 without prior U-Pb dating, initial ε_{Hf} values were only calculated where the zircon
424 U-Pb age is known to be uniform for the population. The initial ε_{Hf} values of the
425 granite and granodiorite samples GGU312610 (3288 Ma), GGU312611 (~3260 Ma),
426 GGU312631 (~3260 Ma) and GGU312696 (3294 Ma) form a scatter between ~ -4
427 and +3 (Fig. 7; with 2σ precision typically in the order of one epsilon unit). In detail,
428 their spread and average initial ε_{Hf} values is; GGU312610 (average= +0.0,
429 maximum= +1.5, minimum= -1.6), GGU312611 (average= +0.1, maximum= +2.3,
430 minimum= -1.4), 312631 (average= -0.9, maximum= +1.8, minimum= -3.8 – without

431 an outlier at +8.2) and GGU312696 (average= -0.1, maximum= +1.3, minimum=
432 -0.6). Due to the more disturbed nature of the zircons in migmatite sample 312630
433 and the non-uniform age of its grains, initial ε_{Hf} values of only four analyses are
434 plotted in figure 7 – those with known U-Pb ages. A greater number of sites with Hf
435 isotopic measurements on zircons without U-Pb age determinations are presented only
436 in Table 3. The two ~3290 Ma grains (1.1, 4.1) yield initial ε_{Hf} values of ~0, whereas
437 the two older sites (2.1, 3.1) yield slightly negative initial e_{Hf} values (Fig. 7).
438 For the metasedimentary samples schist GGU312630 and quartzite GGU312658
439 the zircon age-Hf isotopic data are congruent, and therefore they are treated together.
440 The rarer older 3000-2900 Ma grains yield positive initial e_{Hf} values clustered at ~+5,
441 with two outliers, but both with positive initial values (Table 3, Fig. 7). The dominant
442 ~2710 Ma grains in the samples have a spread in initial e_{Hf} values from ~+0.4 to –10
443 (Table 3, Fig. 7).
444
445 **7. Discussion**
446 *7.1. Geological evolution of the Victoria Fjord basement*
447 Despite the small data set of geochemical and isotopic analyses, and the
448 reconnaissance nature of the field studies of the Victoria Fjord terrane, the integrated
449 field, petrographic, geochemical, geochronological and zircon Hf isotope data provide
450 some robust constraints on the terrane's evolution. This allows the Victoria Fjord
451 terrane to be placed in an Arctic-wide context.
452 For the granitic *sensu lato* rocks it is observed that those with only 3360-3390 Ma

453 magmatic zircons are overall structurally simple, with only a single, often weak
454 foliation defined by biotite ± muscovite. Geochemically these rocks are evolved, with
455 SiO_2 >70 wt% and with high total alkalis, with broadly granodioritic composition.
456 Combined with these features, they display primitive mantle normalised trace element
457 signatures typical of calc-alkali arc related rocks, and in discrimination plots such as
458 Nb+Y – Rb they fall in the upper part of the volcanic arc granite (VAG) field (Fig.
459 2B). The migmatite sample GGU312630 has similar bulk composition (Table 1),
460 however it is observed that its paleosome bands contain hornblende (not observed in
461 the homogeneous granitoids), and the neosomes are hornblende free. This sample also
462 yielded zircons with different ages. Regretfully, because of the strongly metamict
463 nature of the zircons, this is only indicated in a cursory fashion, but even so,
464 oscillatory-zoned magmatic-like grains of ~3500 and 3290 Ma are present (Fig. 5).
465 This, along with results from migmatite sample GGU312632 reported in Nutman et al.
466 (2008a), indicates that the orthogneisses of the Victoria Fjord terrane are dominated
467 by ~3260-3290 Ma intrusions containing a smaller earlier Paleoarchean (3500-3400
468 Ma) crustal component. This probably takes the form of paleosome in the migmatite.
469 The initial ε_{Hf} (t-zircon) values of the 3260-3290 Ma homogeneous metagranitoid
470 rocks (GGU312610, -611, -631 and -696) scatter from ~+3 to -4, beyond analytical
471 uncertainty (Table 3, Fig. 7). The fewer Hf isotopic analyses on the migmatite sample
472 GGU312630 shows that the initial ε_{Hf} values of ~zero for the ~3300 Ma (neosome?)
473 zircons falls in the middle of the range seen for the homogeneous metagranitoid rocks,
474 whereas there are negative initial ε_{Hf} values for the ~3400 and ~3500 Ma grains

475 (Table 3; Fig. 7). The Hf isotopic results on the migmatite lend strong support to a
476 mixed source for the 3260-3290 Ma metagranitoids.
477 Before identifying these contributing sources, it is first necessary to review the
478 temporal Hf isotopic evolutionary trends of potential source reservoirs. A model
479 widely applied in assessing the sources of ancient rocks is a linear evolution of the
480 depleted mantle from CHUR (i.e., $\varepsilon_{Hf} = 0$) at 4560 Ma (Earth's accretion) to ~+17-18
481 at present (the proxy for the upper mantle given by modern MORB). In such a model,
482 juvenile crust extracted from the depleted mantle at 4000 and 3000 Ma (the entire Eo-
483 and Paleoarchean) would display a rise from ~+3 to ~+6 (Fig. 7). However, as
484 examined in detail by Bennett et al., (2007) and Bennett and Nutman (2015), this
485 model scenario does not fit the available Eoarchean data. In fact, initial ε_{Hf} values for
486 juvenile Eoarchean arc-related tonalites and quartz diorites (e.g., Hiess et al., 2009;
487 Hiess and Bennett, 2016) and arc-like tholeiitic basalts (Hoffmann et al., 2011) are all
488 within error of CHUR (i.e. $\varepsilon_{Hf} \approx$ zero), rather than lying on a trend of increasing
489 positive values. It is only during the Paleoarchean (e.g., $\varepsilon_{Hf} = +1$ for the North Atlantic
490 Craton 3200 Ma Akia terrane rocks of Næraa et al. 2012) that the measured initial ε_{Hf}
491 values become positive in juvenile crustal granitoids. This vector, which is faithful to
492 the measured data on ancient juvenile crustal rocks, is portrayed on figure 7 as solid
493 grey lines with arrows. The differences between the linear depleted mantle evolution
494 and the authentic one based on measured initial ε_{Hf} values diminishes in time, such
495 that in the Phanerozoic it has little consequence on calculated depleted mantle (DM)
496 model ages (Bennett and Nutman, 2015). However, disparity between DM model ages

497 will be greatest in the early Archean, with, in the case of the old component in
498 migmatite GGU312630, the linear DM model overestimates extraction from a mantle
499 reservoir by about 100 million years (Table 3 – compare the t-CHUR versus t-DM
500 model ages). Applying the observed depleted mantle ε_{Hf} evolution vector of Bennett
501 and Nutman (2015), the spread of the initial ε_{Hf} values for the 3290-3260 Ma
502 granodiorites can be interpreted as mixtures of a juvenile mantle-derived component
503 (~+2) and an early Paleoarchean crustal component (~-5 to -6 at 3290 Ma). Based on
504 the entire geochemical and isotopic evidence, we interpret the 3260-3290 Ma
505 granodioritic rocks as a calc-alkaline suite, formed in an arc-like environment with
506 mixed juvenile depleted mantle and recycled older Paleoarchean crustal sources. As
507 such, they might represent a late Paleoarchean Andean-style arc built on older
508 Paleoarchean crust (Fig. 8a).

509 The metasedimentary rocks intercalated with the Paleoarchean meta-granitoids are
510 a diverse assemblage of quartzites, metapelites (now mica-garnet schists) and marbles
511 (Henriksen and Jepsen, 1985). The detrital zircon populations of both samples are
512 dominated by Neoarchean (~2710 Ma) grains, with a few Mesoarchean (3000-2900
513 Ma) grains. Most noticeable, despite 40 detrital zircons dated, is the absence of
514 Paleoarchean zircon matching the ages of the intercalated orthogneisses (Fig. 6). This
515 indicates there is no proximal provenance, and that the zircons in these rocks have
516 come from sources not identified in the exposed Victoria Fjord terrane.

517 Integrating the Th/U of the detrital zircons with their initial ε_{Hf} values provides
518 additional insight into the two detrital sources. For the 3000-2900 Ma zircons, the data

519 form a cluster centred on moderate Th/U (~0.5), a value typical for silica-saturated
520 granitoids, and positive ε_{Hf} values of ~+3 (Fig. 9). This initial ε_{Hf} value coincides with
521 the Bennett and Nutman (2015) proposed early Archean depleted mantle trajectory,
522 and therefore we interpret that the 3000-2900 Ma grains were derived from a felsic
523 juvenile crustal component of that age. For the ~2700 Ma zircons, there is a
524 poorly-defined negative correlation between Th/U and ε_{Hf} with r= -0.47 (Fig. 9). High
525 Th/U values of ≥1.0 are normally found in igneous zircons in mafic to intermediate
526 rocks (e.g., Paces and Miller, 1991; Nutman and Ehlers, 1998). In which case, the
527 contributing source to the igneous zircons is *unlikely* to be remelting of strongly
528 negative ε_{Hf} Paleoarchean granitic *sensu lato* crust, where crystallisation of lower
529 Th/U (~0.5-0.3) zircon would be expected. Instead, we propose that these zircons
530 formed from a mafic melt extracted from long-established (Paleoarchean?) enriched
531 lithospheric mantle, that interacted with and assimilated juvenile 3000-2900 Ma
532 continental crust during its ascent (Fig. 8b). These results are compatible with the
533 different REE and trace element chemistry of the two paragneiss samples, for which it
534 is proposed that there were both mafic-intermediate and felsic sources (section 5.2).
535
536 *7.2. Relationship of the Victoria Fjord terrane and the Paleoproterozoic Inglefield*
537 *mobile belt*
538 South of the Victoria Fjord terrane, the Paleoproterozoic Inglefield Mobile Belt
539 (2000-1950) Ma juvenile arc complex occurs on Greenland's most northern west coast.
540 The southern edge of the Inglefield Mobile Belt is in tectonic contact with an Archean

541 gneiss complex and quartzites and marbles of a Paleoproterozoic passive margin
542 (Nutman et al., 2008a and references therein). Similarly, on the east coast, Caledonian
543 allochthonous basement inliers contain juvenile 2000-1950 Ma crust, south of which
544 are Archean gneisses (e.g., Steiger et al., 1979; Kalsbeek et al., 1993). In
545 Independence Fjord (Fig. 1 inset), within the most northeastern part of Greenland
546 where basement is entirely covered by post-Paleoproterozoic sedimentary sequences,
547 the Independence Fjord Group contains abundant ~2000, 2700 and lesser amounts of
548 ~3000 and 3300 Ma detrital zircons (Kirkland et al., 2009). With the current
549 directions mostly from the northeast in these rocks (Kirkland et al., 2009), the
550 provenance of these detrital zircons is likely to be from an easterly continuation of the
551 Victoria Fjord terrane and the Inglefield Mobile Belt (Fig. 1 inset).
552 In the Inglefield Mobile Belt Paleoproterozoic arc assemblage, formation of the
553 2000-1950 Ma arc rocks is followed immediately by high-grade metamorphism,
554 recorded by metamorphic zircon overgrowths with U-Pb ages of ~1920 Ma (Nutman
555 et al., 2008a), and K-Ar hornblende ages from 1880 to 1760 Ma (Larsen and Dawes,
556 1974) show high-grade metamorphism. This is interpreted to indicate that by 1920 Ma,
557 extinction of the arc by consumption of oceanic crust and collision with Archean
558 continental crust.
559 In the Victoria Fjord terrane, the youngest-known granitic rocks are ~3260 Ma,
560 whereas the depositional age of the paragneisses is unknown, apart from the fact that
561 it must be <2700 Ma, the age of the youngest detrital zircons (Fig. 6). The
562 sedimentary rocks have metamorphic assemblages dominated by chlorite, biotite and

563 primary muscovite ± garnet, but without metamorphic segregations forming within
564 them. Also of note, particularly for schist sample GGU312653, no metamorphic
565 zircon overgrowths broad enough for analysis are present. This indicates that
566 metamorphic temperatures were not significantly above ~500ºC, i.e., uppermost
567 greenschist facies or lowermost amphibolite facies. The homogeneous Paleoarchean
568 granodioritic rocks preserve relics of igneous texture and display a single biotite
569 foliation. Likewise, they do not contain young (post-Paleoarchean) metamorphic
570 zircon. This indicates a relatively simple post-3260 Ma tectonothermal history, again
571 without experiencing high-grade metamorphism.

572 Because of the extensive Arctic Platform cover and the Inland Ice, there is no
573 exposed contact between the Paleoproterozoic Inglefield Mobile Belt arc assemblage
574 and the Victoria Fjord terrane. Therefore, their relationship must be gleaned by
575 comparing their chronological and lithologic histories. The first important observation
576 is that the ages of rocks and detrital zircons are entirely incongruent; in the Victoria
577 Fjord terrane meta-granitoids have Paleoarchean (3260-3290 Ma) ages and the
578 youngest detrital zircons are ~2710 Ma, whereas in the Inglefield Mobile Belt ages of
579 all rocks and detrital zircons are Paleoproterozoic – mostly 2000-1950 Ma, apart from
580 a few 1800-1700 Ma late kinematic crustally-derived granites (Nutman et al., 2008a).
581 The only thing common between them is Paleoproterozoic metamorphism known
582 from zircon U-Pb and K-Ar mineral data in the Inglefield Mobile belt (Larsen and
583 Dawes, 1974; Nutman et al., 2008a) and K-Ar hornblende data in the Victoria Fjord
584 terrane (Hansen et al., 1987). Therefore, we propose that they represent unrelated,

585 allochthonous terranes, docked in a Paleoproterozoic tectonothermal event (Fig. 8b).

586

587 *7.3. Archean crustal provinces of Greenland*

588 South of the Inglefield Mobile Belt, early Precambrian Greenland consists of a
589 series of Archean basement crustal blocks, separated by Paleoproterozoic mobile belts
590 that contain sutures marked by relics of arcs, and, in some instances, evidence of
591 transient high pressure metamorphism, eclogites and high-pressure granulites
592 (Kalsbeek, 1981, 1986; Kalsbeek et al., 1987; Kalsbeek and Nutman, 1996; Nutman et
593 al., 2008b; Müller et al., 2018). There is extensive U-Pb zircon geochronology on the
594 Archean basement crustal blocks, particularly on the West Greenland exposures of the
595 North Atlantic Craton between the Nagssugtoqidian (1.85 Ga, Fig. 1 inset) and
596 Ketilidian (1.8 Ga, Fig. 1 inset) Paleoproterozoic orogens. However, there is also a
597 growing database on the Archean domains north of the Nagssugtoqidian orogen.

598 All of these Greenland Archean domains have abundant Mesoarchean (<3200 Ma)
599 to late Neoarchean (~2500 Ma) granitoids, which mark several cycles of crust
600 formation via emplacement of voluminous tonalites with juvenile Sr, Nd and Hf
601 isotopic signatures, followed by high temperature recycling with generation of
602 crustally-derived granites (e.g., Moorbath, 1975; Taylor et al., 1980; Friend et al.,
603 2009; Næraa et al., 2012). Similar cycles of crustal formation and recycling in the
604 Eoarchean has been recognised in considerable detail from the 3900-3600 Ma Itsaq
605 Gneiss Complex of the North Atlantic Craton (e.g., Baadsgaard et al., 1986; Bennett
606 et al., 1993, 2007; Nutman et al., 1996, 2015; Hiess et al., 2009, 2011). North of the

607 Nagssugtoqidian orogen in the Scoresby Sund region of East Greenland, remnants of
608 Eoarchean crust have been discovered in a basement inlier of the Caledonian orogen
609 (Johnston and Kylander-Clark, 2013). Based on the small amount of data acquired on
610 these east Greenland Eoarchean rocks so far, they too show a similar crustal evolution
611 history to the Itsaq Gneiss Complex.

612 There are smaller volumes of late Mesoarchean rocks present in Greenland south
613 of the Inglefield Mobile belt, such as ~3180 and ~3220 Ma oldest components in the
614 Akia terrane of the Nuuk region (e.g., Garde et al., 2001). However, in all these
615 basement complexes, there appears to be a gap in the igneous rock record from ~3225
616 Ma up to ~3600 Ma – spanning most of the Paleoarchean. This is the age of the
617 Victoria Fjord terrane granodioritic rocks and the migmatite components within them.
618 This contrast is demonstrated by a compilation of all U-Pb zircon Archean rock ages
619 from between the northern margin of the Nagssugtoqidian orogen and the southern
620 margin of the Inglefield mobile belt (Fig. 10a).

621 The profile of Greenland Archean crustal ages can also be imaged from the age
622 spectrum of detrital zircons in meta-sedimentary sequences (probably representing
623 tectonised passive margins) along the exteriors of the Paleoproterozoic mobile belts.
624 These are also lacking in detritus derived from Paleoarchean crust (Fig. 10b), as
625 illustrated by data from quartzites on the southern margin of the Inglefield mobile belt
626 (Nutman et al., 2008a), the Karat Group north of the Nagssugtoqidian orogen
627 (Kalsbeek et al., 1998), quartzites at the southern edge of the Nagssugtoqidian orogen
628 (Nutman et al., 1999) and metasedimentary rocks on the northern margin of the

629 Ketilidian orogen (supplementary data Table 3). Therefore, based on current
630 knowledge, to the south of the Inglefield Mobile belt, ~3600-3250 Ma Paleoarchean
631 crust is rare to absent in Greenland.
632
633 *7.4. Early Precambrian crust in the Arctic basin*
634 The Arctic basin contains the northwards propagation of the Atlantic mid-ocean
635 ridge, leading into far northeast Siberia (Fig. 11; Grantz et al., 1990; Pease & Coakley,
636 2018 and references therein). Associated with this is a marked extension of the
637 adjacent continental crust, with the development of a series of Mesozoic and younger
638 sedimentary basins separated by submarine ridges or rises (Pease & Coakley, 2018
639 and references therein). A grab sample of orthogneiss off the side of the Alpha Ridge
640 (Fig. 11; on the Laurentian – easternmost Siberian side of the propagating mid-ocean
641 ridge) yielded a SHRIMP U-Pb zircon age of 3452 ± 13 Ma (Presnyakov et al., 2014),
642 who interpreted this sample as exposed basement. However, it is open to debate
643 whether this sample is *in situ* basement or ice-rafted debris, given that reconstructions
644 of Arctic lithosphere generally regard the Alpha ridge as a Cretaceous large igneous
645 province (summarized by Pease et al., 2014). There has also been sampling of
646 numerous Phanerozoic sedimentary rocks across the Arctic Basin (e.g., Bue &
647 Andresen, 2013; Presnyakov et al., 2014), from which ages of Archean zircons cluster
648 in the Paleoarchean (3500-3400 Ma), and at 3100-3000 and ~2700 Ma. Again,
649 despite >4000 individual grains being dated, absent are Eoarchean and 2900-2750 Ma
650 grains, that would match the age of Greenland basement south of the Inglefield

651 Mobile Belt. Therefore, the Arctic Basin Archean age spectrum resembles that
652 encountered in the Victoria Fjord terrane.
653
654 *7.5. Paleoarchean crust in eastern Siberia*
655 The Siberian Craton of eastern Siberia is approximately 400,000 km^2 in extent and
656 is largely covered by Mesoproterozoic to Phanerozoic sedimentary rocks (Rosen and
657 Turkina, 2007 and references therein). The craton consists of diverse assemblages of
658 Archean rocks that had been assembled and juxtaposed before 1800 Ma (Smelov et al.,
659 1998; Rosen and Turkina, 2007). There are two main areas where basement is
660 exposed; the Anabar province (shield) to the north and west and the Aldan province
661 (shield) to the south and east. These are separated by the Akitkan belt that straddles
662 Lake Baikal, and which contains both Archean basement and early Paleoproterozoic
663 rocks. The Akitkan belt is interpreted as marking a ~1900 Ma suture between the
664 Anabar and Aldan shields (Donskaya et al., 2002).
665 In the Sharyzhalgay Uplift, at the southwestern edge of the Anabar craton where it
666 borders the Central Asian Orogenic Belt, there are granulite facies rocks with
667 SHRIMP zircon U-Pb protolith ages of 3386 ± 14 Ma and an older (inherited?)
668 component of 3415 ± 6 Ma (Bibikova et al., 2006). By the same technique, Poller et al.
669 (2005) identified 3347 ± 37 Ma and 3390 Ma orthogneiss protoliths, with granulite
670 facies metamorphism at 1880 ± 27 Ma. In the Daldyn terrane in the more
671 northerly-exposed parts of the Anabar shield, a felsic gneiss has a SHRIMP zircon
672 U-Pb protolith age of 3320 ± 10 Ma (Bibikova et al., 1988).

673 The Aldan shield consists of a western terrane dominated by the Mesoarchean
674 Olekma granite-greenstone terrane and the eastern granulite facies terrane.
675 Representative tonalites of the granite-greenstone terrane have SHRIMP zircon U-Pb
676 protolith ages of 3016 ± 8 and 3006 ± 11 Ma (Nutman et al., 1992). The Olekma
677 granite-greenstone terrane and the eastern granulite facies terrane are separated by a
678 north-south trending orogenic belt (not named), in which there are relict eclogite
679 facies assemblages formed at 1895 ± 4 Ma, indicative of collisional orogeny with
680 crustal thickening at that time (Nutman et al., 1992). The eastern granulite facies
681 terrane contains Paleoarchean protoliths, Paleoproterozoic granitoids and
682 superimposed Paleoproterozoic low pressure (orthopyroxene and plagioclase coexist)
683 granulite facies metamorphism. This is exemplified by SHRIMP zircon U-Pb ages of
684 a migmatite from the Aldan River, which yielded an age of 3335 ± 2 Ma for the
685 protolith and 1947 ±5 Ma for superimposed syn-granulite facies anatexis (Nutman et
686 al., 1992). The results from far-flung localities across the Siberian Craton indicate the
687 widespread occurrence of Paleoarchean crust. From a compilation of whole rock Nd
688 isotopic data (Rosen and Turkina, 2007), it appears that these Paleoarchean crustal
689 remnants represent juvenile additions to the crust at the time they formed, rather than
690 being tectonothermally recycled older (Eoarchean or Hadean) crust. Supporting this
691 conclusion, there are to our knowledge, the only report for ≥3600 Ma detrital zircons
692 from the Siberian Craton is a single grain by Glukhovski et al. (2017).
693
694

7.6. Paleoarchean crust in northern Canada

The Slave Province of the Northwestern Territories, Canada has a complex early Precambrian history, stretching back into the Hadean in the Acasta area (Fig. 11). Although there has been great focus on the rare Hadean rocks, there are also ~3400-3300 Ma Paleoarchean components present, consisting of both in intact rocks of that age (e.g., Bleeker and Davis, 1999), and as detrital components in younger Precambrian sedimentary rocks (e.g., Pietranik et al., 2008).

7.7. Greenland, the Arctic basin and eastern Siberia – northern Canada: A Eurasia-Gondwana-Tethys Ocean model for the Paleoproterozoic

Compilation of the Archean geochronological data from the Victoria Fjord terrane of far north Greenland, the Arctic Basin, and eastern Siberia point to congruence in the age profile for igneous rock formation; with the absence of Eoarchean rocks, presence of 3500-3260 Ma Paleoarchean and 3000-2900 Ma Mesoarchean rocks, the absence of 2850-2750 Ma rocks, the presence of ~2700 Ma rocks and absence of 2700-2500 Ma rocks. For the sake of the ensuing discussion we informally call this assemblage the *polar continent* – as existing at the end of the Archean (Table 4). This stands in stark contrast to the Archean terranes farther south in Greenland, where locally Eoarchean rocks occur, and where, from zircon geochronology, 3500-3250 Ma Paleoarchean activity is absent, and 2850-2750 Ma and 2600-2500 Ma activity is widespread. We informally call this assemblage the *southern continent* – as existing at the end of the Archean (Table 4).

To explain these age distributions of the ancient polar and southern continents and their relationship with Paleoproterozoic arcs in Greenland, we propose a model resembling the Mesozoic-Cenozoic relationship between Gondwana, Eurasia and the Tethys Oceans. The life cycle of the Paleo- and Neotethys oceans involved fragments of Gondwana being transported across the oceans and accreted onto the southern edge of Eurasia (Şengör, 1984; Ricou, 1994; Robertson et al., 1996). This produced Gondwanan continental blocks ranging in size from the Sanandaj-Sirjan Zone (e.g., Fergusson et al., 2016) now in Iran, to the Indian subcontinent now at the Eurasian margin. Transport of Gondwanan continental crust across the oceans was achieved by a combination of rifting and the formation of oceanic crust that was consumed by several subduction zones above which arc complexes formed. These arc complexes now occur as tectonically-disrupted assemblages interspersed with Gondwana continental fragments. These mostly accumulated at the Eurasian margin (Searle et al., 1987; Robertson, 2012; Gibbons et al., 2015), but some are docked with parts of Gondwana, such as the Cretaceous Hasanbag arc at the northeastern edge of the Arabian sub-continent (Ali et al., 2012). The ultimate product of closure of the Tethyian oceans is for the southern fringe of Eurasia to be marked by a collage of Gondwanan continental fragments, interspersed with several arc complexes, each of which was extinguished when there was arc-continental crustal collision.

In the case of the Precambrian history of the polar region, the Archean polar continent (now being dispersed by opening of the Phanerozoic Arctic Ocean) can be likened to Eurasia, whereas the southern continent can be analogous to Gondwana.

739 Fragments of the southern continent, such as the North Atlantic Craton, were
740 transported across one or more Paleoproterozoic oceans, to be docked on the edge of
741 the polar continent, with each Archean fragment separated by tectonically-modified
742 Paleoproterozoic arc complexes. As noted by Nutman et al. (2008a) these arc
743 complexes young southwards through Greenland, such that arc rocks in the Inglefield
744 Mobile belt and its likely continuation in East Greenland are 2000-1950 Ma, those in
745 the Nagssugtoqidian belt are ~1900 Ma, and those in the Ketilidian belt at the
746 southern extremity of Greenland are ~1850 Ma (Hamilton et al., 1999; Garde et al.,
747 2002). Likewise, associated high-grade metamorphism associated with docking
748 against Archean crust becomes younger southwards.
749

750 **8. Conclusions**

751 1) The Victoria Fjord terrane is dominated by Paleoarchean granitic rocks, with
752 intercalations of sedimentary rocks deposited after ~2700 Ma and containing detrital
753 zircon grains derived from ~2710 and 3000-2900 Ma sources.
754 2) The Victoria Fjord terrane correlates with the provenance of Archean detritus and
755 debated outcrops in the Arctic Ocean and with cratons in eastern Siberia. Its age
756 profile does not match that of Archean basement farther south in Greenland.
757 3) The crustal evolution of the Victoria Fjord terrane is unrelated with that of the
758 Inglefield Mobile Belt to the south, until the onset of a Paleoproterozoic
759 tectonothermal event, probably indicated by the upper greenschist to lowest
760 amphibolite facies assemblages in the metasedimentary intercalations. This indicates

761 Paleoproterozoic docking of these unrelated units.

762

763 **Acknowledgements**

764 This project was supported by a travel grant from the Faculty of Science, Medicine
765 and Health of the University of Wollongong, the GeoQuEST Research Centre,
766 Hiroshima University, the Australian National University and Julie Hollis of the
767 Bureau of Minerals and Petroleum, The Government of Greenland (Naalakkersuisut).
768 We thank Feiko Kalsbeek and Victoria Pease for comments on early versions of this
769 manuscript. Simon Wilde is thanked for his editorial handling of this manuscript.

770

771 **References**

772 Ali, S. A., Buckman, S., Aswad, K. J., Jones, B. G., Ismail, S. A., Nutman, A. P., 2012.
773 Recognition of Late Cretaceous Hasanbag ophiolite-arc rocks in the Kurdistan region of
774 the Iraqi Zagros Thrust Zone: a missing link in the paleogeography of the closing
775 Neo-Tethys Ocean. Lithosphere 4, 395-410.

776 Baadsgaard, H., Nutman, A.P., Bridgwater, D., 1986. Geochronology and isotopic variation
777 of the early Archaean Amîtsoq gneisses of the Isukasia area, southern West Greenland.
778 Geochimica et Cosmochimica Acta 50, 2173- 2183.

779 Bennett, V., Nutman, A., 2015. A Continuum of Crust Formation Processes,
780 Eoarchean-Phanerozoic.Goldschmidt Abstracts, 2015 261

781 Bennett, V.C., Nutman, A.P., McCulloch, M.T., 1993. Nd isotopic evidence for transient,
782 highly depleted mantle reservoirs in the early history of the Earth. Earth and Planetary
783 Science Letters 119, 299-317.
784 Bennett, V., Brandon, A., Hiess, J., Nutman, A., 2007. Crust- mantle dynamics in the early
785 Earth: The $^{142-143}$Nd and ^{176}Hf isotopic perspective. Geochimica et Cosmochimica Acta,
786 71(15) Supplement 79.
787 Bibikova, E.V., Belov, A.N., Rosen, O.M., 1988. Metamorphic rocks isotope dating in the
788 Anabar shield. In: Markov, M.S. (Ed.), Archean of the Anabar Shield and problems of
789 the Early Earth's Evolution. Nauka, Moscow, pp. 122-133 (in Russian).
790 Bibikova, E.V., Turkina, O.M., Kirnozova, T.I., Fugzan, M.M., 2006. Ancient plagiogneisses
791 of the Onot block of the Sharyzhalgay metamorphic massif: isotopic geochronology.
792 Geochemistry International 44, 310-316.
793 Black, L.P., Kamo, S.L., Allen, C.M., Aleinikoff, J.M., Davis, D.W., Korsch, R.J., Foudoulis,
794 C., 2003. TEMORA 1: A new zircon standard for Phanerozoic U-Pb geochronology.
795 Chemical Geology 200, 155–170.
796 Bleeker. W., Davis, W., 1999. The 1991–1996 NATMAP Slave Province Project:
797 introduction. Canadian Journal of Earth Sciences 36 1033-1042.
798 Bouvier, A., Vervoort, J.D., Patchett, J., 2008. The Lu–Hf and Sm–Nd isotopic composition
799 of CHUR: constraints from unequilibrated chondrites and implications for the bulk
800 composition of the terrestrial planets. Earth and Planetary Sciences Letters 273, 48-57.

Bue, E.P., Andresen, A., 2013. Constraining depositional models in the Barents Sea region using detrital zircon U–Pb data from Mesozoic sediments in Svalbard. Geological Society, London, Special Publications 386, 261-279.

Connelly, J.N., van Gool, J.A.M., Mengel, F.C., 2000. Temporal evolution of a deeply eroded orogen; the Nagssugtoqidian Orogen, West Greenland. Canadian Journal of Earth Sciences 37, 1121–1142.

Cumming, G.L., Richards, J.R., 1975. Ore lead ratios in a continuously changing Earth. Earth and Planetary Science Letters, 28, 155-171.

Dawes, P.R., 1976. Precambrian to Tertiary of northern Greenland. In: Escher, A., Watt, W.S. (Eds.), Geology of Greenland, 248–303. Geological Survey of Greenland, Copenhagen, Denmark.

Dawes, P.R., 1978. Crystalline basement complex of the Victoria Fjord arch. Unpublished report, Geological Survey of Greenland, Copenhagen, Denmark, 6 pp.

Dawes, P.R., 2006. Explanatory notes to the geological map of Greenland, 1:500 000, Thule, Sheet 5. Geological Survey of Denmark and Greenland Map Series 2, 97 pp.

Dawes, P.R., 2009. The bedrock geology under the Inland Ice: the next major challenge for Greenland mapping. Geological Survey of Denmark and Greenland Bulletin 17, 57-60.

Dawes, P.R., Frisch, T., 1981. Geological reconnaissance of the Greenland Shield in Melville Bugt, North-West Greenland. Rapport Grønlands Geologiske Undersøgelse 105, 18–26.

Dawes, P.R., Larsen, O., Kalsbeek, F., 1988. Archean and Proterozoic crust in North-West Greenland: evidence from Rb–Sr whole-rock age determinations. Canadian Journal of Earth Sciences 25, 1365–1373.

823 Dawes, P.R., Frisch, T., Garde, A.A., Iannelli, T.R., Ineson, J.R., Jensen, S.M., Pirajno, F.,
824 Sønderholm, M., Stemmerik, L., Stouge, S., Thomassen, B., van Gool, J.A.M., 2000.
825 Kane Basin 1999: mapping, stratigraphic studies and economic assessment of
826 Precambrian and Lower Palaeozoic provinces in north-western Greenland. Geology of
827 Greenland Survey Bulletin 186, 11–28.
828 Donskaya, T.V., Salnikova, E.B., Sklyarov, E.V., 2002. Early Proterozoic post-collision
829 magmatism at the southern flank of the Siberian Craton: new geochronological data and
830 geodynamic implication. Doklady Earth Sciences 383, 125-128.
831 Fergusson, C, Nutman, A.P., Mohajjel, M., Bennett, C., 2016. The Sanandaj-Sirjan Zone in
832 the Neo-Tethyan suture, western Iran: zircon U-Pb evidence of late Palaeozoic rifting of
833 northern Gondwana and mid Jurassic orogenesis. Gondwana Research 40, 43-57.
834 Friend, C.R.L., Nutman, A.P., Baadsgaard, H., Duke, J., 2009. The whole rock Sm-Nd 'age'
835 for the 2825 Ma Ikkattoq gneisses (Greenland) is 800 Ma too young: Insights into
836 Archaean TTG petrogenesis. Chemical Geology 261, 61-75.
837 Garde, A.A., Friend, C.R.L., Marker, M., Nutman, A.P., 2001. Rapid maturation and
838 stabilisation of middle Archaean continental crust: the Akia terrane, southern West
839 Greenland. Bulletin of the Geological Society of Denmark 47, 1-27.
840 Garde, A.A., Hamilton, M.A., Chadwick, B., Grocott, J., McCaffrey, K.J.W., 2002. The
841 Ketilidian orogen of South Greenland: geochronology, tectonics, magmatism, and
842 fore-arc accretion during Palaeoproterozoic oblique convergence. Canadian Journal of
843 Earth Sciences 39, 765–793.

GGU, 1970. Tectonic/geological map of Greenland, 1:2 500 000. Geological Survey of Greenland, Copenhagen, Denmark.

Gibbons, A.D., Zahirovic, S., Müller, R.D., Whittaker, J.M., Yatheesh, V., 2015. A tectonic model reconciling evidence for the collisions between India, Eurasia and intra-oceanic arcs of the central-eastern Tethys. Gondwana Research 28, 451–492.

Glukhovskii, M.Z., Kuz'min, M.I., Bayanova, T.B., Lyalina, L.M., Makrygin, V.A., Shcherbakova, T.F., 2018. The First Discovery of Hadean Zircon in Garnet Granulites from the Sutam River (Aldan Shield). Doklady Earth Sciences 476, 1026-1032.

Grantz, A., Johnson, L., Sweeney, J.F. (Eds), 1990. The Arctic Ocean Region. The Geology of North America, L. Geological Society of America, Boulder, Colorado, 644 pp.

Grantz, A., Hart, P., Childers, V., 2011. Geology and tectonic development of the Amerasia and Canada Basins, Arctic Ocean. In: Spencer, A.M., Embry, A.F., Gautier, D.L., Stoupakova, A.V., Sørensen, K. (Eds.), Arctic Petroleum Geology. Geological Society (London) Memoirs, 35, 771–799.

Haller, J., 1961. An account of Caledonian orogeny in Greenland. In Raasch, G.O. (Ed.), Geology of the Arctic 1, 170–187. University Press, Toronto.

Hamilton, M.A., Garde, A.A., Chadwick, B., Grocott, J., McCaffrey, K., 1999. Temporal evolution of the Palaeoproterozoic Ketilidian orogen, South Greenland: a synopsis of results from conventional and SHRIMP U–Pb geochronology. European Union of Geosciences, 10th Annual meeting, Journal of Conference Abstracts 4(1), 129.

Hansen, B.T., Kalsbeek, F., Holm, P.M., 1987. Archaean age and Proterozoic metamorphic overprinting of the crystalline basement at Victoria Fjord, North Greenland. Rapport Grønlands Geologiske Undersøgelse 133, 159–168.

Henriksen, N., Jepsen, H.F., 1985. Precambrian crystalline basement at the head of Victoria Fjord, North Greenland. Rapport Grønlands Geologiske Undersøgelse 126, 11–16.

Hiess, J., Bennett, V.C., 2016. Chondritic Lu/Hf in the early crust-mantle system as recorded by zircon populations from the oldest Eoarchean rocks of Yilgarn Craton, West Australia and Enderby Land, Antarctica. Chemical Geology 427, 125-143.

Hiess, J., Bennett, V.C., Nutman, A.P., Williams, I.S., 2009. In situ U-Pb, O and Hf isotopic compositions of zircon from Eoarchaean tonalite and felsic volcanic rocks, Itsaq Gneiss Complex, southern West Greenland: New constraints on the source materials for the early crust. Geochimica et Cosmochimica Acta 73, 4489-4516.

Hiess J., Bennett V. C., Nutman A. P., Williams I. S., 2011. Archaean fluid-assisted crustal cannibalism recorded by low δ18O and negative εHf(T) isotopic signatures of West Greenland granite zircon: Contributions to Mineralogy and Petrology, 101, 1027-1050.

Hoffmann, J.E., Münker, C., Polat, A., Rosing, M.T., Schulz, T., 2011. The origin of decoupled Hf–Nd isotope compositions in Eoarchean rocks from southern West Greenland. Geochimica et Cosmochimica Acta 75, 6610-6628.

Hurst, J.M., Peel, J.S., 1979. Late Proterozoic(?) to Silurian stratigraphy of southern Wulff Land, North Greenland. Rapport Grønlands Geologiske Undersøgelse 91, 37–56.

Johnston, S.M., Kylander-Clark, A.R.C., 2013. Discovery of an Eo-Meso-Neoarchean terrane in the East Greenland Caledonides. Precambrian Research 235, 295-302.

886 Kalsbeek, F., 1981. The northward extent of the Archaean basement of Greenland – a review
887 of Rb–Sr whole-rock ages. Precambrian Res. 14, 203–219.
888 Kalsbeek, F., 1986. The tectonic framework of the Precambrian shield of Greenland. A review
889 of new isotopic evidence. In: Kalsbeek, F., Watt, W.S. (Eds.), Developments in
890 Greenland geology. Rapport Grønlands Geologiske Undersøgelse 128, 55–64.
891 Kalsbeek, F., Nutman, A.P., 1996. Anatomy of the Early Proterozoic Nagssugtoqidian
892 orogen, West Greenland, explored by reconnaissance SHRIMP U–Pb zircon dating.
893 Geology 24(6), 515–518.
894 Kalsbeek, F., Pidgeon, R.T., Taylor, P.N., 1987. Nagssugtoqidian mobile belt of West
895 Greenland: a cryptic 1850 Ma suture between two Archaean continents--chemical and
896 isotopic evidence. Earth and Planetary Science Letters 85, 365-385.
897 Kalsbeek, F., Nutman, A.P., Taylor, P.N., 1993. Palaeoproterozoic basement province in the
898 Caledonian fold belt of North-East Greenland. Precambrian Res. 63, 163–178.
899 Kalsbeek, F., Pulvertaft, T.C.R., Nutman, A.P., 1998. Geochemistry, age and origin of
900 metagreywackes from the Palaeoproterozoic Karrat Group, Rinkian Belt, West
901 Greenland. Precambrian Res. 91, 383–39.
902 Kirkland, C.L., Pease, V., Whitehouse, M.J., Ineson, J.R., 2009. Provenance record from
903 Mesoproterozoic-Cambrian sediments of Peary Land, North Greenland: Implications
904 for the ice-covered Greenland Shield and Laurentian palaeogeography. Precambrian
905 Research 170, 43-60.

Larsen, O., Dawes, P.R., 1974. K/Ar and Rb/Sr age determinations on Precambrian crystalline rocks in the Inglefield Land – Inglefield Bredning region, Thule district, western North Greenland. Rapport Grønlands Geologiske Undersøgelse 66, 4–8.

Ludwig, K.R., 2003. Isoplot 3.0: A geochronological toolkit for Microsof Excel. Berkeley Geochronological Center Special Publication 4. Berkeley Geochronological Center, Berkeley, California. 70 pp.

McDonough, W.F., Sun, S.S., 1995. The composition of the Earth. Chemical Geology 120, 223–253.

Moorbath, S., 1975, Evolution of Precambrian crust from strontium isotopic evidence: Nature, v. 254, p. 395-398.

Müller, S., Dziggel, A., Kolb, J., Sindern, S., 2018. Age and temperature-time evolution of retrogressed eclogite-facies rocks in the Paleoproterozoic Nagssugtoqidian Orogen, South-East Greenland: Constrained from U-Pb dating of zircon, monazite, titanite and rutile. Precambrian Research, 314, 468-486.

Nance, R. D., Murphy, J. B., Santosh, M., 2014. The supercontinent cycle: a retrospective essay. Gondwana Research 25, 4–29.

Norrish, K., Chappell, B.W., 1977. X-ray fl uorescence spectrometry, in Zussman, J., ed., Physical Methods of Determinative Mineralogy (2nd ed.): London, Academic Press, p. 201–272.

Nutman, A.P., 1984. Precambrian gneisses and intrusive anorthosite of Smithson Bjerge, Thule district, North-West Greenland. Rapport Grønlands Geologiske Undersøgelse 119, 31 pp.

928 Nutman, A.P., Ehlers, K., 1998. Evidence for multiple Palaeoproterozoic thermal events and
929 magmatism adjacent to the Broken Hill Pb-Zn-Ag orebody, Australia. Precambrian
930 Research 90, 203-238.
931 Nutman, A.P., Kalsbeek, F., 1994. Search for Archaean basement in the Caledonian fold belt
932 of North-East Greenland. In: Higgins, A.K. (Ed.), Geology of North-East Greenland.
933 Rapport Grønlands Geologiske Undersøgelse 162, 129–133.
934 Nutman, A.P., Kalsbeek, F., 1999. SHRIMP U-Pb zircon ages for Archaean granitoid rocks,
935 Ataa area, north-east Disko Bugt, West Greenland. Geology of Greenland Survey
936 Bulletin 181, 49-54.
937 Nutman, A.P., Chernyshev, I.V., Baadsgaard, H., Smelov, A.P., 1992. The Aldan Shield of
938 Siberia, U.S.S.R.: The age of its Archaean components and evidence for widespread
939 reworking in the Mid Proterozoic. Precambrian Research 54, 195-210.
940 Nutman, A.P., McGregor, V.R., Friend, C.R.L., Bennett, V.C., Kinny, P.D., 1996. The Itsaq
941 Gneiss Complex of southern West Greenland; the world's most extensive record of
942 early crustal evolution (3900–3600 Ma). Precambrian Research 78, 1–39.
943 Nutman, A.P., Kalsbeek, F., Marker, M, van Gool, J.A.M., Bridgwater, D., 1999. U–Pb zircon
944 ages of Kangâmiut dykes and detrital zircons in metasediments in the Palaeoproterozoic
945 Nagssugtoqidian Orogen (West Greenland). Clues to the pre-collisional history of the
946 orogen. Precambrian Res. 93, 87–104.
947 Nutman, A.P., Dawes, P., Kalsbeek, F., Hamilton, M.A., 2008a. Palaeoproterozoic and
948 Archaean gneiss complexes in northern Greenland: Palaeoproterozoic terrane assembly
949 in the High Arctic. Precambrian Research, 161, 419-451.

950 Nutman, A.P., Kalsbeek, K. & Friend, C.R.L., 2008b. The Nagssugtoqidian orogen in
951 South-East Greenland: Evidence for Paleoproterozoic collision and plate assembly.
952 American Journal of Science 308, 529-572.
953 Nutman, A.P., Bennett, V.C., Friend, C.R.L., 2015. Proposal for a continent 'Itsaqia'
954 amalgamated at 3.66 Ga and rifted apart from 3.53 Ga: Initiation of a Wilson cycle near
955 the start of the rock record. American Journal of Science 315, 509-536.
956 Næraa, T., Scherstén, A., Rosing, M.T., Kemp, A.I.S., Hoffmann, J.E., Kokfelt, T.F.,
957 Whitehouse, M.J., 2012. Hafnium isotope evidence for a transition in the dynamics of
958 continental growth 3.2 Gyr ago. Nature 485, 627-631.
959 Paces, J.B., Miller, J.D. Jr., 1993. Precise U-Pb ages of Duluth Complex and related mafic
960 intrusions, northeastern Minnesota: Geochronological insights to physical, petrogenetic,
961 paleomagnetic, and tectonomagmatic processes associated with the 1.1 Ga midcontinent
962 rift system. Journal of Geophysical Research 98, 13997–140013.
963 Pease, V., Coakley, B., 2018. Circum-Arctic lithosphere evolution. Geological Society,
964 London, Special Publications 460, 1-6.
965 Pease, V., Drachev, S., Stephenson, R., Zhang, X., 2014. Arctic lithosphere – A review.
966 Tectonophysics 628, 1-25.
967 Pietranik, A.B., Hawkesworth, C.J., Storey, C.D., Kemp, A.I.S., Sircombe, K.N.,
968 Whitehouse, M.J., Bleeker, W., 2008. Episodic, mafic crust formation from 4.5 to 2.8
969 Ga: New evidence from detrital zircons, Slave craton, Canada. Geology 36, 875-878.
970 Poller, U., Gladkochub, D., Donskaya, T., Mazukabzov, A., Sklyarov, E., Todt, W., 2005.
971 Multistage magmatic and metamorphic evolution in the Southern Siberia craton:

Archean and Palaeoproterozoic ages revealed by SHRIMP and TIMS. Precambrian Research 136, 353-368.

Presnyakov, S., Sergeev, S., Antonov, A., Belyatsky, B., Rodionov, N., Shevchenko, S., 2014. Paleo- and Mesoarchean zircon from Arctic Ocean bottom rocks: an indicator of vintage continental crust. In 7th International SHRIMP Workshop Abstracts, National Institute of Polar Research, 32-37.

Ricou, L.E., 1994. Tethys reconstructed: plates, continental fragments and their boundaries since 260 Ma: From Central America to South-eastern Asia. Geodynamica Acta 7, 169–218.

Robertson, A.H.F, 2012. Late Palaeozoic–Cenozoic tectonic development of Greece and Albania in the context of alternative reconstructions of Tethys in the Eastern Mediterranean region. International Geology Review 54, 373-454.

Robertson, A.H.F., Dixon, J.E., Brown, S., Collins, A., Morris, A., Pickett, E., Sharp, I., Ustaömer, T., 1996. Alternative tectonic models for the Late Palaeozoic–Early Tertiary development of Tethys in the Eastern Mediterranean region. In: Morris, A., Tarling, D.H. (Eds.), Palaeomagnetism and Tectonics of the Mediterranean Region. Geological Society of London Special Publication 105, 239–263.

Rogers, J. J. W., 1996. A history of continents in the past three billion years. Journal of Geology 104, 91–107,

Rosen, O.M., Turkina, O.M., 2007. The oldest rock assemblages of the Siberian craton. In: Van Kranendonk, M.J., Smithies, R.H., & Bennett, V.C. (eds) Earth's Oldest Rocks. Elsevier, pp. 793-838.

994 Scherer, E., Munker, C., Mezger, K., 2001. Calibration of the lutetium–hafnium clock.
995 Science 293, 683-687. doi:10.1126/science.1061372.
996 Schjøth, F., Steenfelt, A., Thorning, L. (Eds.), 1996. Regional compilations of geoscience data
997 from Inglefield Land, North-West Greenland. Thematic Map Series Grønlands
998 Geologiske Undersøgelse 96/1, 35 pp. + 51 maps.
999 Searle, M.P., Windley, B.F., Coward, M.P., Cooper, D.J.W., Rex, A.J., Rex, D., Li, T.D.,
1000 Xiao, X.C., Jan, M.Q., Thakur, V.C., Kumar, S., 1987. The closing of Tethys and the
1001 tectonics of the Himalaya. Geological Society of America Bulletin 98, 678–701.
1002 Şengör, A.M.C., 1984. The Cimmeride orogenic system and tectonics of Eurasia. Geological
1003 Society of America Special Paper 195 (82 pp.).
1004 Smelov, A.P., Zedgenizov, A.,N., Parfenov, L.M., Timofeev, V.F., 1998. Precambrian
1005 terranes of the Aldan-Stanovoi shiled: In Metallogeny, Petroleum Potential, and
1006 Geodynamics of the North Asian Craton and the Surrounding Orogenic Belts. Santai
1007 Publ., Irkutsk, pp. 119-120 (in Russian).
1008 Steenfelt, A., Dam, E., 1996. Reconnaissance geochemical mapping of Inglefield Land,
1009 North-West Greenland. Danmarks og Grønlands Geologiske Undersøgelse Rapport
1010 1998/12, 27 pp. + 49 maps.
1011 Steiger, R.H., Hansen, B.T., Schuler, C., Bär, M.T., and Henriksen, N., 1979, Polyorogenic
1012 nature of the southern Caledonian fold belt in East Greenland. Journal of Geology, v. 87,
1013 p. 475-495.
1014 Söderlund, U., Patchett, P.J., Vervoort, J.D., Isachsen, C.E., 2004. The 176Lu decay constant
1015 determined by Lu–Hf and U–Pb isotope systematics of Precambrian mafic intrusions.

1016 Earth and Planetary Science Letters 219, 311-324.
1017 doi:10.1016/S0012-821X(04)00012-3.
1018 Taylor, S.R. and McClennan, S.M., 1985. The Continental Crust: Its Composition and
1019 Evolution. Geoscience Texts, Blackwell, Oxford.
1020 Taylor, P.N., Moorbath, S., Goodwin, R., Petrykowski, A.C., 1980. Crustal contamination as
1021 an indicator of the extent of early Archaean continental crust: Pb isotopic evidence from
1022 the late Archaean gneisses of West Greenland. Geochimica et Cosmochimica Acta 44,
1023 1427-1453.
1024 Thomassen, B., Dawes, P.R., 1996. Inglefield Land 1995: geological and economic
1025 reconnaissance in North-West Greenland. Bulletin Grønlands Geologiske Undersøgelse
1026 172, 62–68.
1027 Thomassen, B., Dawes, P.R., Steenfelt, A., Krebs, J.D., 2002. *Qaanaaq 2001*: mineral
1028 exploration reconnaissance in North-West Greenland. Geology of Greenland Survey
1029 Bulletin 191, 133–143.
1030 Thrane, K., 2002. Relationships between Archaean and Palaeoproterozoic crystalline
1031 basement complexes in the southern part of the East Greenland Caledonides: an ion
1032 microprobe study. Precambrian Research 113, 19-42.
1033 Trettin, H.P. (Ed.), 1991. Geology of the Innuitian Orogen and the Arctic Platform of Canada
1034 and Greenland. Geology of Canada 3, 569 pp. + map vol. Geological Survey of Canada,
1035 Ottawa, Ontario. (Also: The geology of North America E, Geological Society of
1036 America, Boulder, Colorado.)

1037 Whitehouse, M.J., Kalsbeek, F., Nutman, A.P., 1998. Crystal growth and crystal recycling in
1038 the Nagssugtoqidian orogen of West Greenland: constraints from radiogenetic isotopic
1039 systematics and U–Pb zircon geochronology. Precambrian Res. 91, 365–381.
1040 Williams, I.S., 1998. U-Th-Pb geochronology by ion microprobe. In: Applications of
1041 microanalytical techniques to understanding mineralizing processes. In: McKibben,
1042 M.A., Shanks III, W.C.P., Ridley, W.I., (Eds.), Soc. Econ. Geol. Short Course vol. 7.
1043 Zegers, T.E., de Wit, M.J., Dann, J., White, S.H., 1998. Vaalbara, Earth's oldest assembled
1044 continent? A combined structural, geochronological, and palaeomagnetic test: Terra
1045 Nova 10, 250-259.
1046

Figures

Figure 1. Geological sketch map of the Victoria Fjord terrane (after Henriksen and Jepsen, 1985), with the inset showing the position in Greenland. The 1.85 Ga belt is the Nagssugtoqidian orogen and 1.8 Ga belt is the Ketilidian orogen.

Figure 2. (a) SiO_2 – Zr/Ti; (b) Rb – Y+Nb plots for Victoria Fjord terrane granitic rocks.

Figure 3. (a) REE plot for granitoids normalised using the chondrite values of Taylor and McClennan (1985); (b) REE plot for the sedimentary rocks, normalised using the post-Archean average shale (PAAS) values of Taylor and McClennan (1985); (c) trace element plot for granitoids normalised using the primitive mantle values of McDonough and Sun (1995).

Figure 4. Representative cathodoluminescence images of dated zircons. The high-resolution images were taken after undertaking the LA-ICP-MS Hf isotope analyses, hence the large, deep craters that are present. $^{207}Pb/^{206}Pb$ ages are given at 1 σ uncertainty. Initial ε_{Hf} values of sites are given in brackets.

Figure 5. Zircon $^{238}U/^{206}Pb$ – $^{207}Pb/^{206}Pb$ concordia diagrams for Victoria Fjord terrane granitic *sensu lato* rocks. Analytical errors shown at the 2σ level.

Figure 6. $^{238}U/^{206}Pb$ – $^{207}Pb/^{206}Pb$ concordia diagram for Victoria Fjord terrane detrital zircons in sedimentary rocks. Analytical errors shown at the 2σ level. The side panel shows the cumulative frequency age distribution, with most grains having Neoarchean, a few having Mesoarchean ages, and none matching the age of the adjacent (basement) granitoid rocks.

1069 Figure 7. Initial ε_{Hf} plot versus zircon age plot for rocks from the Victoria Fjord terrane.

1070 Figure 8. Set of cartoon cross sections depicting the early Precambrian geological

1071 evolution of the Victoria Fjord terrane.

1072 Figure 9. Detrital zircon initial ε_{Hf} versus Th/U plot for rocks from the Victoria Fjord

1073 terrane.

1074 Figure 10. Ages for (a) Archean samples located between the Inglefield and

1075 Nagssugtoqidian Mobile Belts (Nutman and Kalsbeek, 1999; Thrane et al., 2002;

1076 Nutman et al., 2008a,b; Johnston and Kylander-Clark, 2013; R.T. Pidgeon unpublished

1077 data in Nutman et al., 2008a). (b) Archean detrital zircons in Paleoproterozoic clastic

1078 sedimentary rocks throughout Greenland (Kalsbeek et al., 1998; Nutman et al., 1999,

1079 2008a,b; supplementary data).

1080 Figure 11. Map (base from Creative Commons copyright-free resources:

1081 https://creativecommons.org.au/) over the Arctic Basin and the adjoining lands. The

1082 solid green line in Greenland marks the southern limit of 3.5-3.25 Ga Paleoarchean

1083 rocks in Greenland. North of that line, rocks occur in both northernmost Greenland

1084 (Victoria Fjord terrane), as detritus and disputed basement outcrops (extended, rifted

1085 continental crust) in the Arctic Ocean and as outcrops in eastern Siberia (Anabar Shield

1086 and eastern Aldan Shield). The scenario proposed in this paper is that the latter regions

1087 are part of a Precambrian continent, which contains one or more 3.5-3.25 Ga nuclei.

1088

1089 **Tables**

1090 Table 1. Whole rock geochemical analyses of Victoria Fjord terrane rocks.

1091 Table 2. SHRIMP zircon U-Pb analyses of Victoria Fjord terrane rocks.

1092 Table 3. Summary LA-ICP-MS zircon Hf isotopic analyses of Victoria Fjord terrane

1093 rocks. See supplementary Table 1 for more comprehensive data, including standard

1094 analyses.

1095 Table 4. Age profiles of the polar and southern continents.

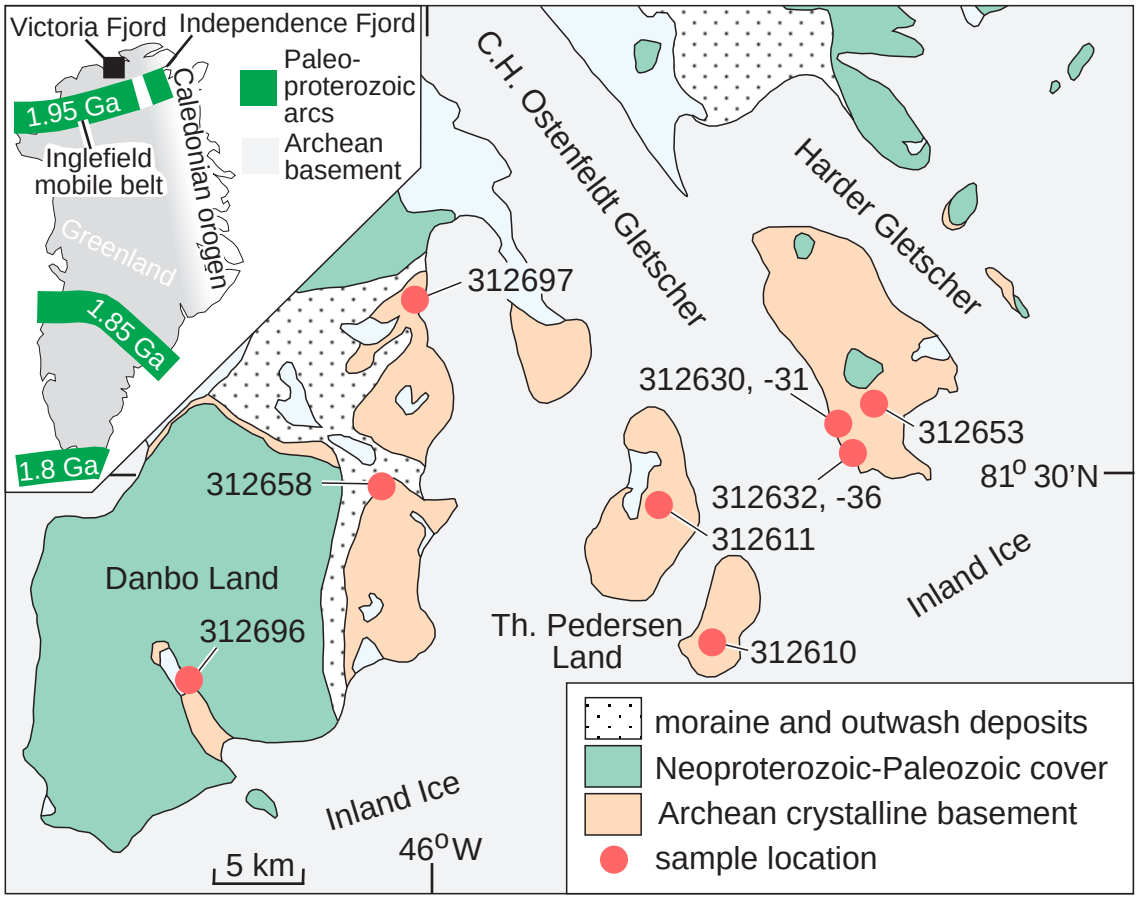
Victoria Fjord
Independence Fjord
1.95 Ga
Inglefield mobile belt
Caledonian orogen
Paleo-proterozoic arcs
Archean basement
Greenland
1.85 Ga
1.8 Ga
C.H. Ostenfeldt Gletscher
Harder Gletscher
312697
312630, -31
312653
81° 30'N
312658
312632, -36
312611
Inland Ice
Danbo Land
312696
Th. Pedersen Land
312610
Inland Ice
46°W
5 km
moraine and outwash deposits
Neoproterozoic-Paleozoic cover
Archean crystalline basement
sample location

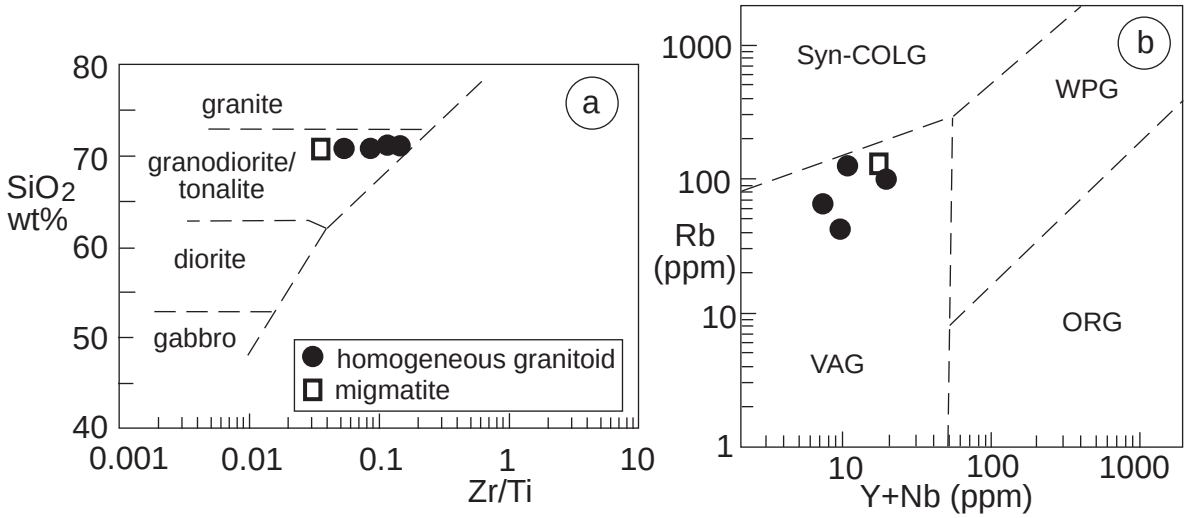
a
granite
granodiorite/
tonalite
diorite
gabbro
homogeneous granitoid
migmatite
SiO2
wt%
80
70
60
50
40
0.001
0.01
0.1
1
10
Zr/Ti
b
Syn-COLG
WPG
ORG
VAG
Rb
(ppm)
1000
100
10
1
10
100
1000
Y+Nb (ppm)

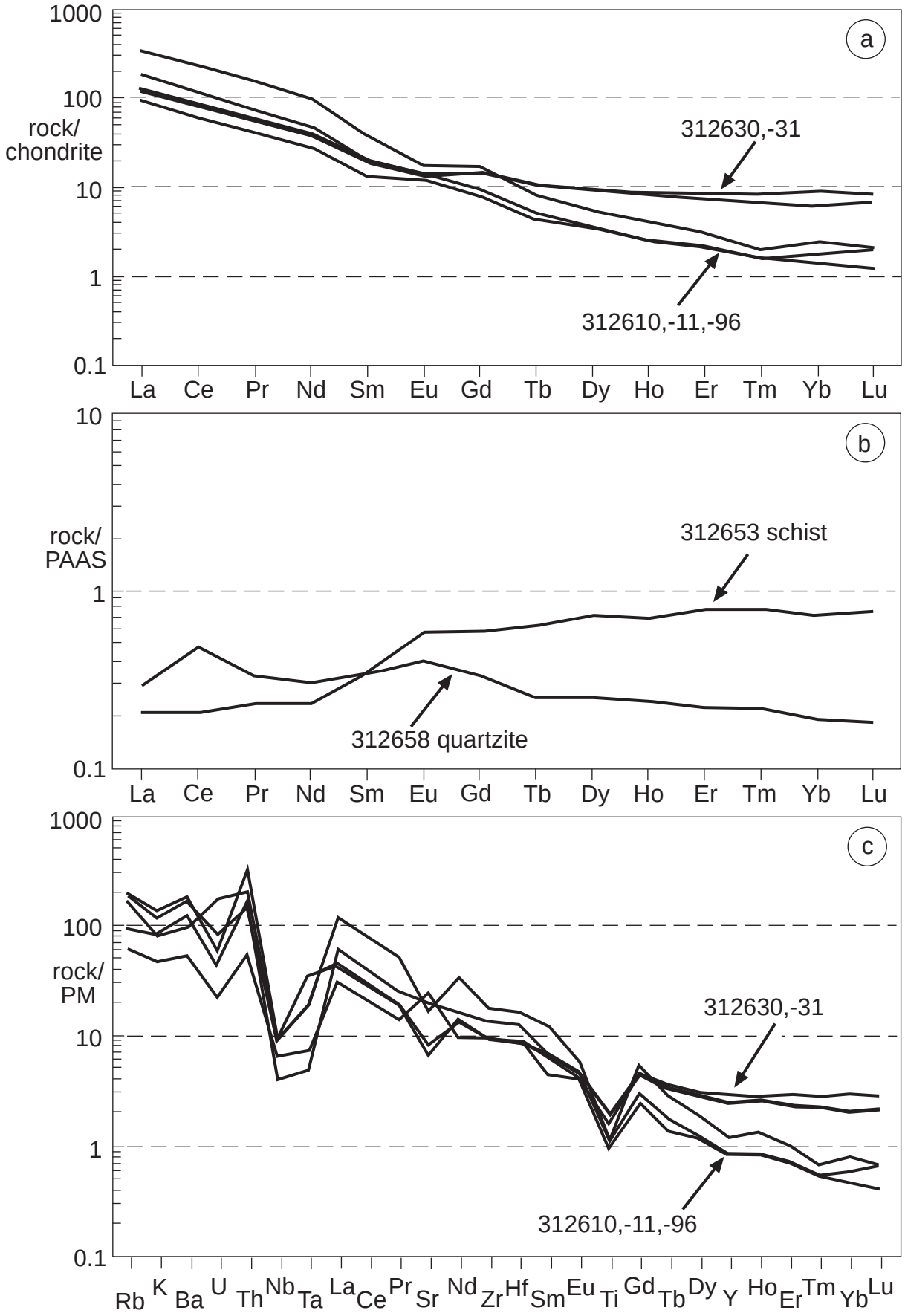
a
1000
100
10
1
0.1
rock/
chondrite
312630,-31
312610,-11,-96
La Ce Pr Nd Sm Eu Gd Tb Dy Ho Er Tm Yb Lu
b
10
1
0.1
rock/
PAAS
312653 schist
312658 quartzite
La Ce Pr Nd Sm Eu Gd Tb Dy Ho Er Tm Yb Lu
c
1000
100
10
1
0.1
rock/
PM
312630,-31
312610,-11,-96
Rb K Ba U Th Nb Ta La Ce Pr Sr Nd Zr Hf Sm Eu Ti Gd Tb Dy Y Ho Er Tm Yb Lu

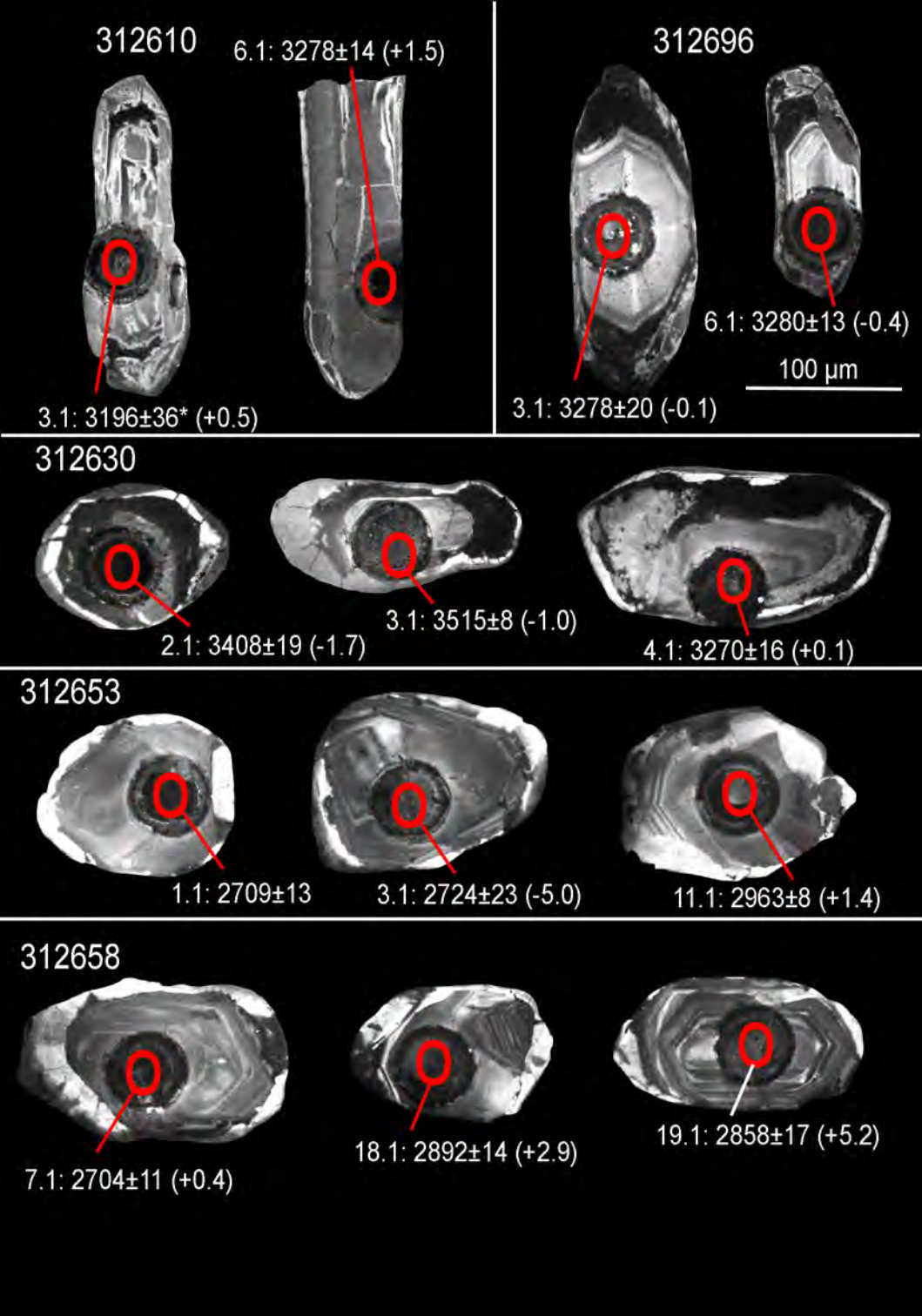
312610
6.1: 3278±14 (+1.5)
3.1: 3196±36* (+0.5)
312696
6.1: 3280±13 (-0.4)
100 µm
3.1: 3278±20 (-0.1)
312630
2.1: 3408±19 (-1.7)
3.1: 3515±8 (-1.0)
4.1: 3270±16 (+0.1)
312653
1.1: 2709±13
3.1: 2724±23 (-5.0)
11.1: 2963±8 (+1.4)
312658
7.1: 2704±11 (+0.4)
18.1: 2892±14 (+2.9)
19.1: 2858±17 (+5.2)

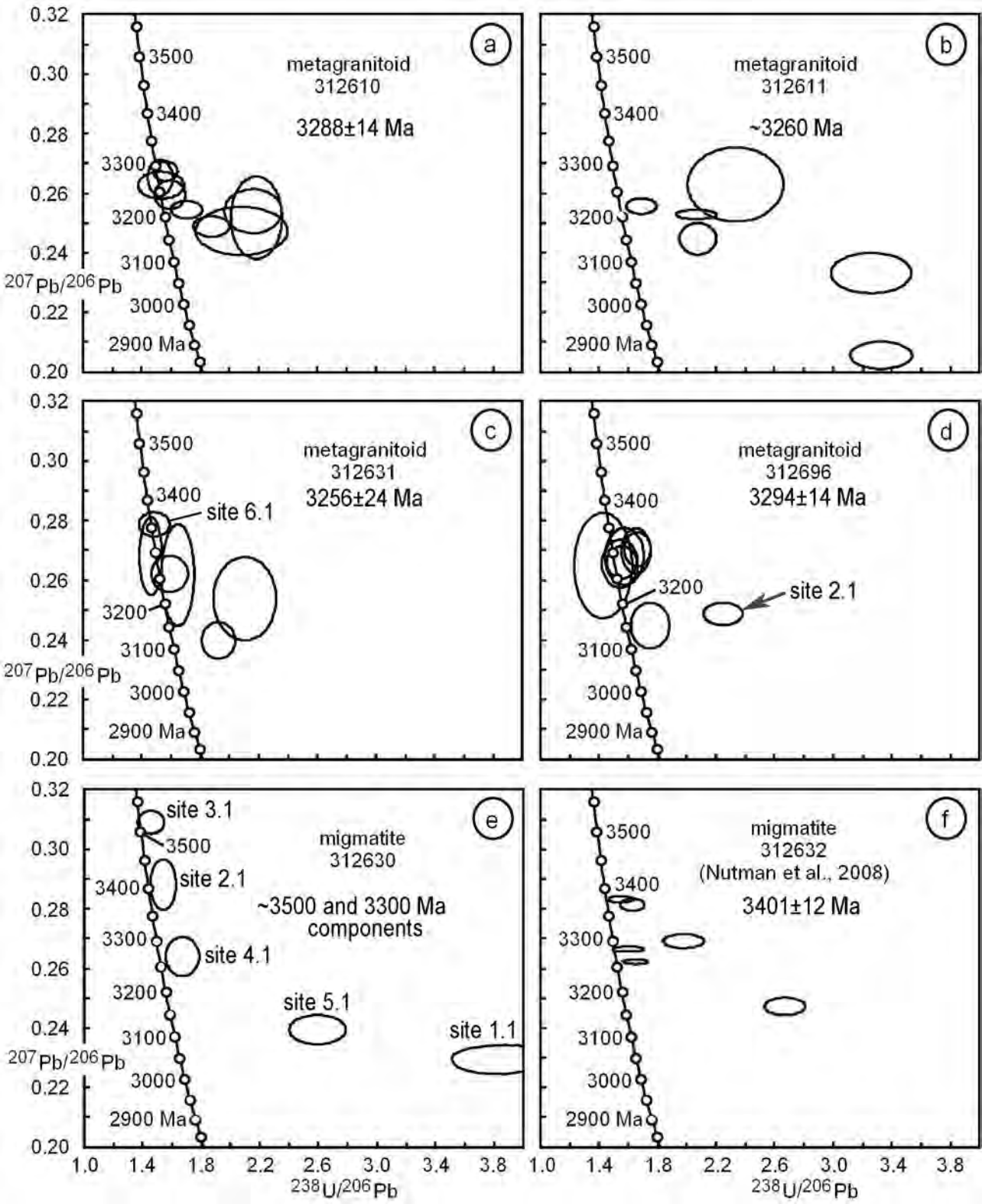
a
metagranitoid
312610
3288±14 Ma
b
metagranitoid
312611
~3260 Ma
c
metagranitoid
312631
3256±24 Ma
site 6.1
d
metagranitoid
312696
3294±14 Ma
site 2.1
e
migmatite
312630
~3500 and 3300 Ma
components
site 3.1
site 2.1
site 4.1
site 5.1
site 1.1
f
migmatite
312632
(Nutman et al., 2008)
3401±12 Ma
3500
3400
3300
3200
3100
3000
2900 Ma
0.32
0.30
0.28
0.26
0.24
0.22
0.20
$^{207}Pb/^{206}Pb$
1.0
1.4
1.8
2.2
2.6
3.0
3.4
3.8
$^{238}U/^{206}Pb$

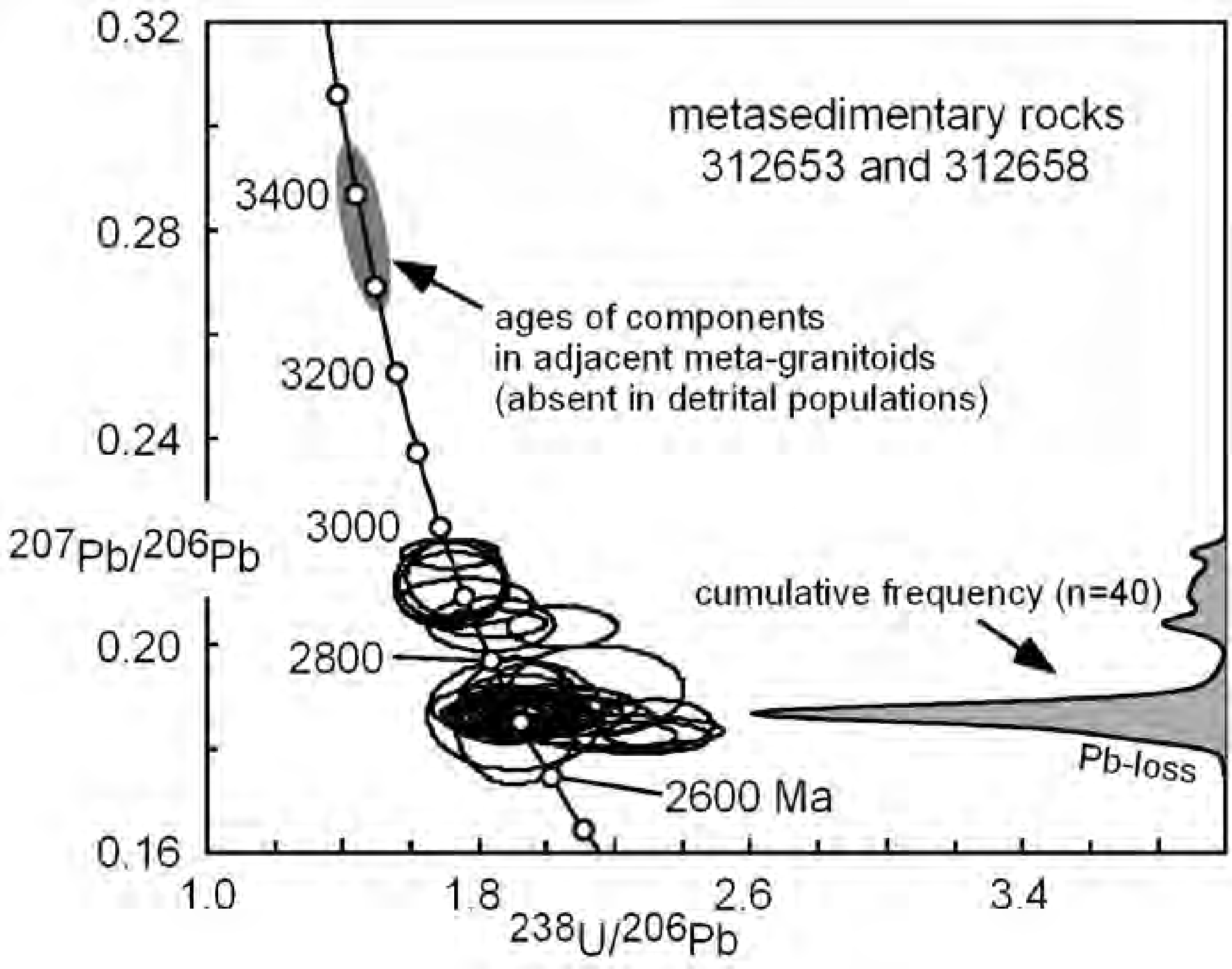
metasedimentary rocks
312653 and 312658
3400
3200
3000
2800
2600 Ma
ages of components
in adjacent meta-granitoids
(absent in detrital populations)
cumulative frequency (n=40)
Pb-loss
0.32
0.28
0.24
0.20
0.16
$^{207}Pb/^{206}Pb$
1.0
1.8
2.6
3.4
$^{238}U/^{206}Pb$

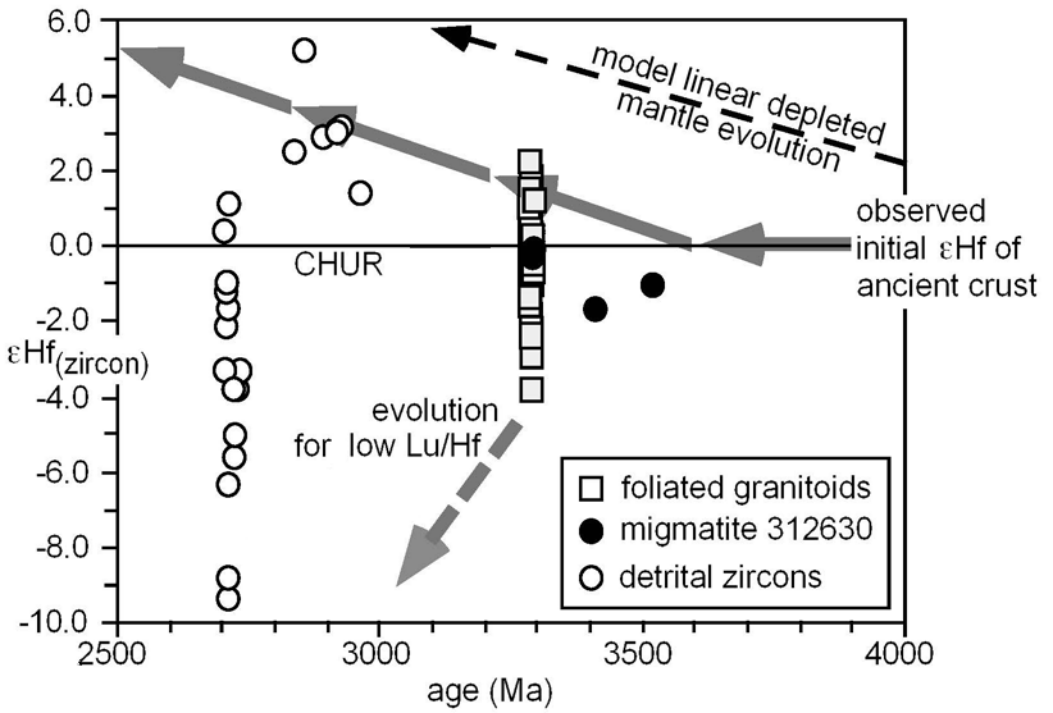
6.0
4.0
2.0
0.0
-2.0
-4.0
-6.0
-8.0
-10.0
εHf(zircon)
2500
3000
3500
4000
age (Ma)
model linear depleted mantle evolution
observed initial εHf of ancient crust
CHUR
evolution for low Lu/Hf
foliated granitoids
migmatite 312630
detrital zircons

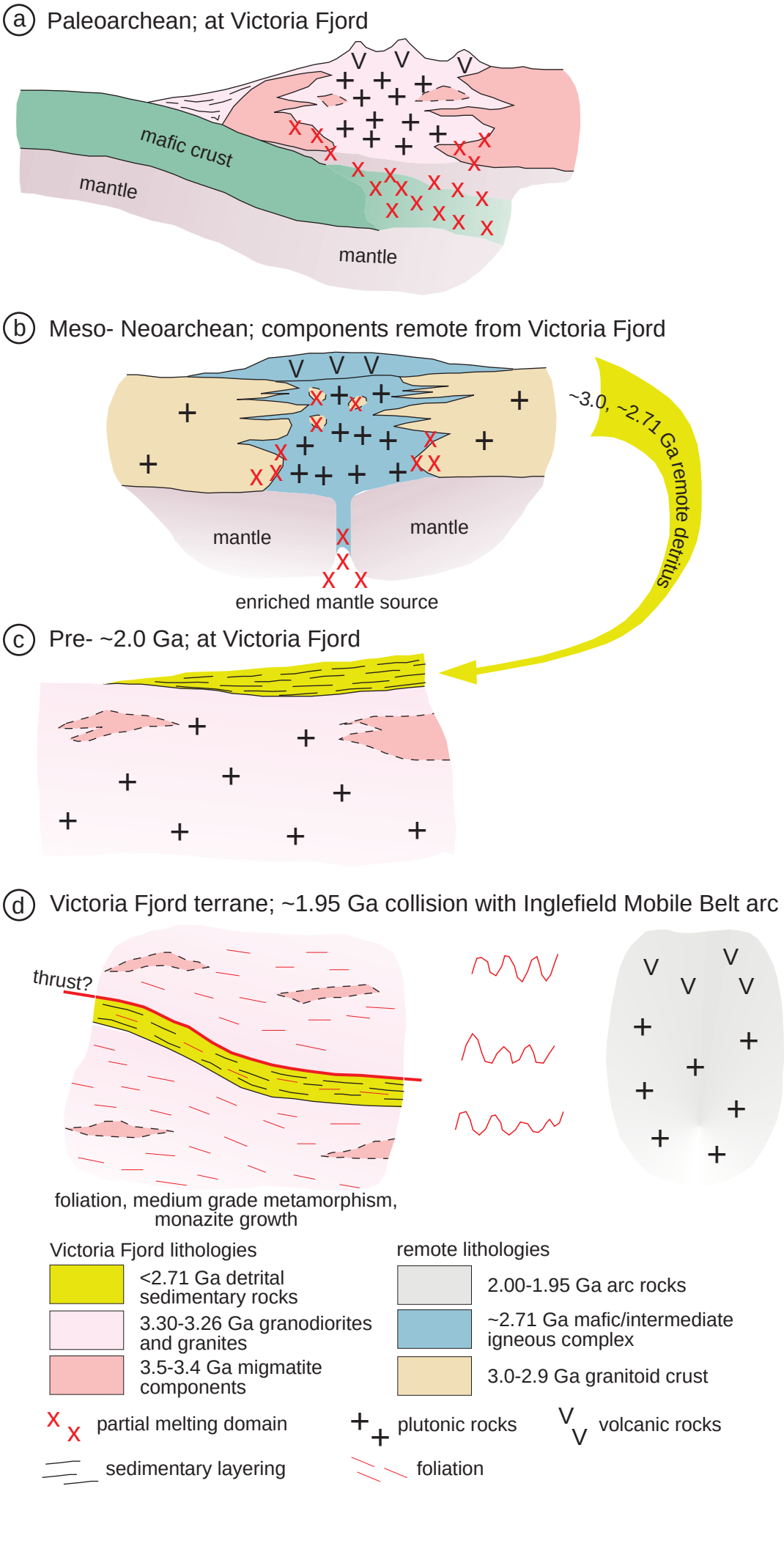
a Paleoarchean; at Victoria Fjord
mafic crust
mantle
mantle
b Meso- Neoarchean; components remote from Victoria Fjord
mantle
mantle
enriched mantle source
~3.0, ~2.71 Ga remote detritus
c Pre- ~2.0 Ga; at Victoria Fjord
d Victoria Fjord terrane; ~1.95 Ga collision with Inglefield Mobile Belt arc
thrust?
foliation, medium grade metamorphism, monazite growth
Victoria Fjord lithologies
<2.71 Ga detrital sedimentary rocks
3.30-3.26 Ga granodiorites and granites
3.5-3.4 Ga migmatite components
remote lithologies
2.00-1.95 Ga arc rocks
~2.71 Ga mafic/intermediate igneous complex
3.0-2.9 Ga granitoid crust
partial melting domain
plutonic rocks
volcanic rocks
sedimentary layering
foliation

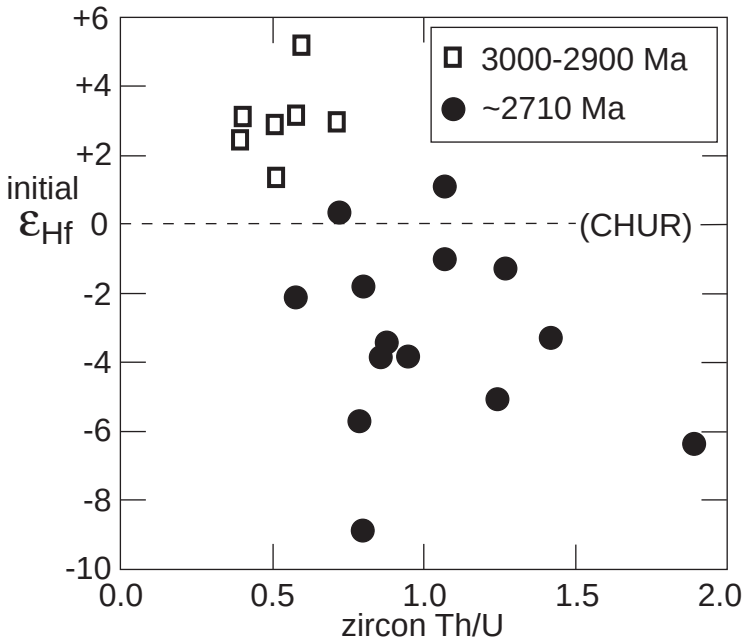
+6
+4
+2
initial
εHf 0
-2
-4
-6
-8
-10
(CHUR)
3000-2900 Ma
~2710 Ma
0.0
0.5
1.0
1.5
2.0
zircon Th/U

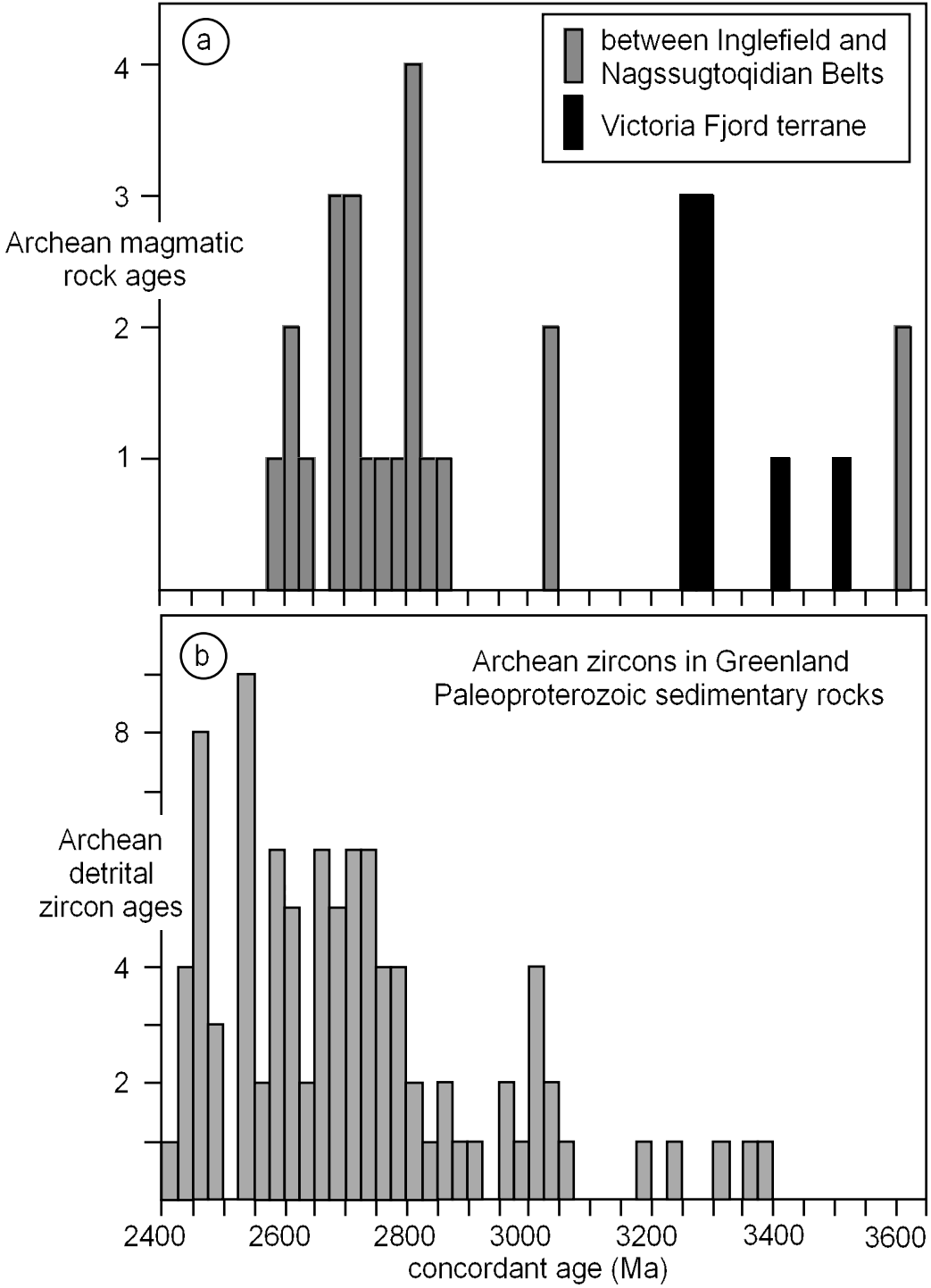
a
between Inglefield and Nagssugtoqidian Belts
Victoria Fjord terrane
Archean magmatic rock ages
4
3
2
1
b
Archean zircons in Greenland Paleoproterozoic sedimentary rocks
Archean detrital zircon ages
8
4
2
2400
2600
2800
3000
3200
3400
3600
concordant age (Ma)


eastern Aldan Shield
Anabar Shield
Acasta
Canada
Russia
Arctic Ocean
Alpha ridge
?
polar continent
mid-ocean ridge
No 3550-3250 Ma crust south of this line in Greenland
Victoria Fjord
Greenland
southern continent
180°W/E
0°W/E
90°W
90°E
80°N
70°N
localities with 3500-3250 Ma crust

Table 2. SHRIMP zircon U-Pb and reconnaissance monazite Pb-Pb analyses

labels	site	U	Th	Th/U	comm	$^{238}U/^{206}Pb$	$^{207}Pb/^{206}Pb$	$^{238}U/^{206}Pb$	$^{207}Pb/^{206}Pb$	%conc
		ppm	ppm		206%	ratio	ratio	date (Ma)	date (Ma)	
GGU312610 metagranite 3288±14 Ma (MSWD=0.62)										
1.1	e,hd,p,fr	714	87	0.121	0.48	1.877 ± 0.051	0.2489 ± 0.0014	2753 ± 62	3178 ± 9	87
2.1	m,hd,p	1795	340	0.190	0.27	2.161 ± 0.080	0.2540 ± 0.0030	2452 ± 76	3210 ± 19	76
3.1	e,hd,p,fr	1255	194	0.155	0.48	2.183 ± 0.071	0.2518 ± 0.0057	2431 ± 66	3196 ± 36	76
4.1	m,hd,p	718	72	0.101	0.27	1.593 ± 0.043	0.2595 ± 0.0020	3140 ± 67	3243 ± 12	97
5.1	m,hd,p	598	328	0.549	0.34	1.562 ± 0.034	0.2674 ± 0.0014	3190 ± 55	3291 ± 8	97
6.1	e,hd,p,fr	475	57	0.121	1.42	1.526 ± 0.035	0.2652 ± 0.0024	3248 ± 59	3278 ± 14	99
7.1	e,hd,p	347	72	0.208	0.51	1.532 ± 0.063	0.2627 ± 0.0019	3238 ± 106	3263 ± 11	99
8.1	m,hd,p,fr	839	64	0.076	0.43	1.706 ± 0.044	0.2545 ± 0.0012	2974 ± 61	3213 ± 8	93
9.1	m,hd,p	580	75	0.129	2.32	2.081 ± 0.129	0.2473 ± 0.0033	2529 ± 131	3168 ± 21	80
GGU312611 metagranite 3250-3300 Ma										
1.1	c?h,p	1443	240	0.166	0.97	3.265 ± 0.112	0.2329 ± 0.0028	1722 ± 52	3072 ± 19	56
2.1	e,osc,p	1236	84	0.068	0.18	2.082 ± 0.051	0.2444 ± 0.0022	2529 ± 52	3149 ± 14	80
3.1	m,osc,p	2845	1454	0.511	0.32	3.333 ± 0.086	0.2053 ± 0.0019	1691 ± 39	2868 ± 15	59
4.1	m,osc,p	1176	87	0.074	0.11	2.072 ± 0.056	0.2525 ± 0.0006	2539 ± 57	3201 ± 4	79
4.2	m,osc,p	677	308	0.455	0.25	2.340 ± 0.133	0.2626 ± 0.0051	2294 ± 111	3262 ± 31	70
5.1	m,hd,p	1013	44	0.043	0.10	1.696 ± 0.042	0.2553 ± 0.0011	2987 ± 60	3218 ± 7	93
GGU312631 metagranite ~3300 Ma										
1.1	e,osc,p,fr	155	104	0.672	0.81	1.462 ± 0.031	0.2677 ± 0.0054	3360 ± 57	3293 ± 32	102
2.1	e,osc,p,fr	92	31	0.336	1.45	2.104 ± 0.087	0.2534 ± 0.0057	2507 ± 87	3206 ± 36	78
3.1	osc,eq	466	1	0.002	0.56	2.951 ± 0.075	0.1285 ± 0.0032	1881 ± 42	2078 ± 45	91
4.1	osc,p,fr	550	339	0.616	0.90	1.924 ± 0.047	0.2395 ± 0.0025	2698 ± 54	3117 ± 17	87
5.1	osc,m,p,fr	95	50	0.523	0.56	1.592 ± 0.051	0.2617 ± 0.0025	3142 ± 80	3257 ± 15	97
6.1	m,osc,p	219	143	0.653	0.15	1.486 ± 0.043	0.2783 ± 0.0017	3318 ± 75	3353 ± 9	99
7.1	m,osc,p	517	219	0.424	1.87	1.648 ± 0.045	0.2614 ± 0.0069	3057 ± 67	3255 ± 42	94
8.1	m,osc,p	755	151	0.199	1.05	4.112 ± 0.151	0.1709 ± 0.0027	1403 ± 46	2566 ± 26	55
GGU312630 migmatite 3250-3300 and ~3500 Ma										
1.1	osc,ov	2022	1136	0.562	0.29	3.857 ± 0.146	0.2296 ± 0.0019	1486 ± 50	3049 ± 13	49
2.1	osc,ov	289	128	0.444	0.56	1.540 ± 0.036	0.2882 ± 0.0035	3225 ± 59	3408 ± 19	95
3.1	m,osc/h,p	198	100	0.505	0.36	1.456 ± 0.038	0.3090 ± 0.0016	3371 ± 68	3516 ± 8	96
4.1	m,osc/h,p	347	115	0.331	0.28	1.672 ± 0.046	0.2639 ± 0.0027	3023 ± 67	3270 ± 16	92
5.1	m,osc/h,eq	918	227	0.247	1.38	2.594 ± 0.079	0.2394 ± 0.0020	2102 ± 55	3116 ± 13	68
GGU312632 migmatite 3401±12 (MSWD=0.10; Nutman et al., 2008)										
1.1	osc,p	1470	429	0.292	0.03	1.549 ± 0.034	0.2831 ± 0.0004	3211 ± 56	3380 ± 2	95
1.2	osc,p	1002	355	0.354	0.06	1.627 ± 0.033	0.2813 ± 0.0008	3089 ± 51	3370 ± 5	92
2.1	osc,p	1037	45	0.044	1.05	2.670 ± 0.057	0.2472 ± 0.0012	2051 ± 38	3167 ± 8	65
3.1	h,rex,p	3283	191	0.058	0.02	1.599 ± 0.044	0.2664 ± 0.0004	3131 ± 68	3285 ± 2	95
3.2	hd,rex,p	3471	200	0.057	1.14	9.011 ± 0.276	0.1174 ± 0.0007	678 ± 20	1917 ± 11	35
3.3	hd,rex,p	7783	1204	0.155	0.63	12.408 ± 0.469	0.0778 ± 0.0007	500 ± 18	1143 ± 18	44
4.1	osc,p	541	44	0.082	0.25	1.977 ± 0.056	0.2691 ± 0.0010	2638 ± 62	3301 ± 6	80
5.1	h,rex,p	2802	157	0.056	0.03	1.649 ± 0.033	0.2622 ± 0.0003	3056 ± 49	3260 ± 2	94
GGU312696 metagranodiorite 3292±14 Ma (MSWD=0.59)										
1.1	c?h,p	145	72	0.497	0.87	1.574 ± 0.054	0.2676 ± 0.0039	3171 ± 87	3292 ± 23	96
2.1	m,h/osc,p	938	357	0.381	1.81	2.248 ± 0.054	0.2484 ± 0.0015	2372 ± 48	3174 ± 10	75
3.1	c?h,p	152	103	0.679	0.97	1.543 ± 0.050	0.2652 ± 0.0033	3221 ± 83	3278 ± 20	98
4.1	c?h,p	147	105	0.714	0.25	1.555 ± 0.042	0.2656 ± 0.0022	3202 ± 68	3280 ± 13	98
5.1	m,h/osc,p	165	83	0.501	0.29	1.428 ± 0.081	0.2645 ± 0.0072	3422 ± 153	3274 ± 44	105
6.1	m,h/osc,p	239	224	0.938	0.26	1.662 ± 0.037	0.2700 ± 0.0023	3037 ± 54	3306 ± 13	92
7.1	e,h,eq	509	63	0.123	0.37	1.749 ± 0.053	0.2445 ± 0.0031	2915 ± 72	3149 ± 20	93
8.1	e,osc,eq,fr	408	146	0.358	0.25	1.653 ± 0.041	0.2695 ± 0.0031	3049 ± 60	3303 ± 18	92
1.0	monazite				<0.01		0.1199 ± 0.0050		1954 ± 76	
2.0	monazite				<0.01		0.1208 ± 0.0056		1967 ± 86	
GGU312653 paragneiss deposited >2000 Ma										
1.1	m,osc	207	237	1.142	0.05	1.835 ± 0.060	0.1862 ± 0.0014	2804 ± 75	2709 ± 13	104
2.1	m,osc	320	266	0.831	0.44	2.278 ± 0.083	0.1822 ± 0.0013	2346 ± 72	2673 ± 11	88
3.1	m,osc	153	191	1.244	0.05	1.919 ± 0.074	0.1879 ± 0.0026	2704 ± 86	2724 ± 23	99
4.1	e,osc	47	90	1.892	0.18	1.909 ± 0.073	0.1853 ± 0.0050	2716 ± 85	2701 ± 45	101
5.1	m,osc	198	261	1.318	0.08	2.048 ± 0.072	0.1865 ± 0.0017	2563 ± 74	2711 ± 15	95
6.1	e,osc	236	188	0.796	1.08	2.318 ± 0.070	0.1846 ± 0.0019	2312 ± 59	2695 ± 17	86
7.1	e,osc	473	377	0.798	0.07	1.935 ± 0.069	0.1868 ± 0.0008	2686 ± 79	2714 ± 7	99
8.1	m,osc	60	24	0.404	0.46	1.712 ± 0.066	0.2115 ± 0.0034	2965 ± 93	2917 ± 26	102
9.1	m,osc	242	96	0.397	0.11	1.837 ± 0.064	0.2042 ± 0.0011	2802 ± 80	2860 ± 9	98
10.1	e,osc	233	134	0.578	0.19	2.002 ± 0.058	0.1860 ± 0.0012	2611 ± 63	2707 ± 11	97
11.1	m,osc	111	57	0.511	0.20	1.715 ± 0.059	0.2176 ± 0.0011	2961 ± 83	2963 ± 8	100
12.1	e,osc	288	249	0.863	0.05	1.970 ± 0.064	0.1883 ± 0.0009	2647 ± 71	2728 ± 8	97
13.1	e,osc	163	207	1.275	0.20	1.860 ± 0.064	0.1858 ± 0.0012	2773 ± 79	2706 ± 11	103
14.1	e,osc	137	102	0.740	0.12	1.926 ± 0.062	0.1864 ± 0.0017	2696 ± 72	2710 ± 15	100
15.1	e,osc	218	169	0.776	0.14	1.942 ± 0.068	0.1882 ± 0.0012	2678 ± 77	2726 ± 10	98
16.1	e,osc	220	231	1.052	0.05	1.886 ± 0.055	0.1875 ± 0.0009	2743 ± 66	2720 ± 8	101
17.1	e,osc	146	154	1.052	0.08	1.931 ± 0.057	0.1872 ± 0.0012	2690 ± 65	2718 ± 11	99
18.1	m,osc	148	86	0.578	0.18	1.734 ± 0.059	0.2129 ± 0.0031	2935 ± 81	2927 ± 24	100
19.1	m,osc	270	332	1.228	0.05	2.034 ± 0.061	0.1876 ± 0.0010	2578 ± 64	2721 ± 9	95
20.1	e,osc	87	98	1.120	0.32	1.951 ± 0.057	0.1890 ± 0.0030	2668 ± 64	2733 ± 27	98
GGU312658 paragneiss deposited >2000 Ma										
1.1	e,osc	102	238	2.340	0.25	2.146 ± 0.105	0.1912 ± 0.0035	2466 ± 101	2753 ± 31	90
2.1	m,osc/h	90	92	1.029	0.24	2.207 ± 0.747	0.1854 ± 0.0028	2409 ± 719	2702 ± 26	89
3.1	m,osc/h	213	304	1.423	0.23	1.984 ± 0.069	0.1859 ± 0.0013	2631 ± 75	2706 ± 12	97
4.1	m,osc	191	205	1.073	0.16	1.874 ± 0.055	0.1865 ± 0.0010	2756 ± 66	2711 ± 9	102
5.1	m,osc	207	223	1.075	0.11	1.873 ± 0.066	0.1862 ± 0.0020	2758 ± 80	2708 ± 18	102
6.1	m,osc	674	386	0.573	0.40	2.191 ± 0.135	0.1834 ± 0.0012	2424 ± 125	2684 ± 11	90
7.1	e,osc	149	108	0.726	0.21	1.918 ± 0.087	0.1857 ± 0.0013	2705 ± 101	2704 ± 11	100

Table 2. SHRIMP zircon U-Pb and reconnaissance monazite Pb-Pb analyses

labels	site	U	Th	Th/U	comm	$^{238}U/^{206}Pb$	$^{207}Pb/^{206}Pb$	$^{238}U/^{206}Pb$	$^{207}Pb/^{206}Pb$	%conc
		ppm	ppm		206%	ratio	ratio	date (Ma)	date (Ma)	
8.1	m,osc	153	134	0.877	0.06	2.017 ± 0.085	0.1892 ± 0.0012	2595 ± 91	2735 ± 10	95
9.1	e,osc	264	248	0.941	0.04	1.920 ± 0.073	0.1887 ± 0.0012	2703 ± 84	2731 ± 10	99
10.1	e,osc	201	159	0.791	0.14	1.869 ± 0.085	0.1876 ± 0.0018	2762 ± 103	2721 ± 16	102
11.1	e,osc	179	348	1.942	0.08	1.945 ± 0.063	0.1866 ± 0.0020	2674 ± 71	2712 ± 18	99
12.1	e,osc	248	240	0.965	0.33	2.087 ± 0.092	0.1862 ± 0.0014	2523 ± 92	2709 ± 13	93
13.1	m,osc	93	93	0.997	0.17	1.881 ± 0.066	0.1860 ± 0.0021	2748 ± 79	2707 ± 18	102
14.1	m,h	54	38	0.711	0.20	1.725 ± 0.067	0.2113 ± 0.0027	2947 ± 92	2916 ± 21	101
15.1	m,osc	114	91	0.800	0.14	1.887 ± 0.076	0.1869 ± 0.0015	2741 ± 91	2715 ± 14	101
16.1	m,osc	456	349	0.766	0.46	2.184 ± 0.082	0.1824 ± 0.0012	2430 ± 76	2674 ± 11	91
17.1	m,osc	498	292	0.585	0.26	1.907 ± 0.106	0.1865 ± 0.0043	2717 ± 124	2712 ± 39	100
18.1	r,h	72	37	0.507	0.09	1.762 ± 0.081	0.2083 ± 0.0018	2898 ± 108	2892 ± 14	100
19.1	m,osc	80	48	0.598	0.06	1.835 ± 0.076	0.2039 ± 0.0021	2804 ± 95	2858 ± 17	98
18.2	m,osc	144	91	0.630	0.29	2.045 ± 0.066	0.2034 ± 0.0016	2566 ± 68	2854 ± 13	90
20.1	e,osc	83	64	0.776	0.11	2.100 ± 0.068	0.1880 ± 0.0015	2511 ± 68	2724 ± 13	92

all uncertainties in the Table are given at 1 sigma

Site: x.y, x=grain number, y=analysis number

Grain and site character: p=prism, eq=small aspect ratio prism, ov=oval, fr=grain fragment
m=middle of grain, c?=possible core, e=edge of grain, r=rim

Cathodoluminescence character: osc=oscilatory zoned, h=homogeneous, hd=dark homogeneous

Common Pb correction: comm 206%= percentage of ^{206}Pb that is non-radiogenic, based on measured ^{204}Pb and common Pb modelled as Cumming and Richards (1975) for likely age of rock

Table 3. Summary of Victoria Fjord zircon Lu-Hf isotopic data.

Sample	$^{174}Hf/^{177}Hf$	$^{178}Hf/^{177}Hf$	$^{176}Lu/^{177}Hf$	Measured $^{176}Hf/^{177}Hf$	εHf(0)[1]	U-Pb age (Ga)	Initial $^{176}Hf/^{177}Hf$	εHf(t)	T(DM)[2] (Ga)
312610 metagranite									
1.1	0.008652 ± 0.000014	1.467447 ± 0.000028	0.001087 ± 0.000051	0.280737 ± 0.000010	-72.41 ± 0.35	3.288	0.28067	0.3	3.35
2.1	0.008653 ± 0.000016	1.467452 ± 0.000040	0.001581 ± 0.000037	0.280749 ± 0.000011	-72.00 ± 0.38	3.288	0.28065	-0.4	3.38
5.1	0.008671 ± 0.000012	1.467478 ± 0.000034	0.000920 ± 0.000024	0.280722 ± 0.000013	-72.94 ± 0.45	3.288	0.28066	0.1	3.36
3.1	0.008656 ± 0.000011	1.467478 ± 0.000031	0.000988 ± 0.000021	0.280736 ± 0.000008	-72.45 ± 0.30	3.288	0.28067	0.5	3.35
4.1	0.008665 ± 0.000013	1.467438 ± 0.000033	0.001075 ± 0.000054	0.280733 ± 0.000011	-72.55 ± 0.37	3.288	0.28067	0.2	3.36
6.1	0.008653 ± 0.000016	1.467501 ± 0.000038	0.000892 ± 0.000027	0.280749 ± 0.000011	-72.00 ± 0.41	3.288	0.28069	1.2	3.32
7.1	0.008716 ± 0.000029	1.467368 ± 0.000369	0.001333 ± 0.000071	0.280787 ± 0.000057	-70.65 ± 2.02	3.288	0.28070	1.5	3.31
8.1	0.008667 ± 0.000011	1.467313 ± 0.000122	0.000646 ± 0.000026	0.280678 ± 0.000018	-74.51 ± 0.63	3.288	0.28064	-0.8	3.39
9.1	0.008656 ± 0.000032	1.467203 ± 0.000058	0.001022 ± 0.000042	0.280680 ± 0.000024	-74.43 ± 0.83	3.288	0.28062	-1.6	3.42
A	0.008623 ± 0.000020	1.467451 ± 0.000027	0.001809 ± 0.000015	0.280758 ± 0.000009	-71.69 ± 0.34	3.288	0.28064	-0.6	3.39
B	0.008660 ± 0.000012	1.467443 ± 0.000036	0.000738 ± 0.000010	0.280704 ± 0.000011	-73.57 ± 0.39	3.288	0.28066	-0.1	3.37
C	0.008657 ± 0.000014	1.467467 ± 0.000031	0.000864 ± 0.000029	0.280734 ± 0.000007	-72.54 ± 0.26	3.288	0.28068	0.7	3.34
D	0.008663 ± 0.000016	1.467410 ± 0.000022	0.001683 ± 0.000063	0.280759 ± 0.000011	-71.64 ± 0.38	3.288	0.28065	-0.3	3.38
E	0.008644 ± 0.000009	1.467449 ± 0.000030	0.000422 ± 0.000011	0.280683 ± 0.000009	-74.34 ± 0.31	3.288	0.28066	-0.1	3.37
312611 metagranite									
5.1	0.008652 ± 0.000015	1.467555 ± 0.000044	0.000715 ± 0.000031	0.280767 ± 0.000009	-71.4 ± 0.33	3.290	0.28072	2.3	3.29
A	0.008664 ± 0.000010	1.467441 ± 0.000030	0.000502 ± 0.000014	0.280678 ± 0.000010	-74.5 ± 0.34	3.290	0.28065	-0.5	3.38
B.1	0.008625 ± 0.000011	1.467436 ± 0.000028	0.001076 ± 0.000020	0.280711 ± 0.000010	-73.4 ± 0.34	3.290	0.28064	-0.6	3.39
B.2	0.008622 ± 0.000011	1.467431 ± 0.000030	0.001057 ± 0.000019	0.280706 ± 0.000010	-73.5 ± 0.35	3.290	0.28064	-0.7	3.39
C	0.008647 ± 0.000005	1.467342 ± 0.000028	0.000849 ± 0.000005	0.280675 ± 0.000007	-74.6 ± 0.24	3.290	0.28062	-1.4	3.42
D	0.008641 ± 0.000012	1.467549 ± 0.000028	0.000454 ± 0.000028	0.280680 ± 0.000011	-74.4 ± 0.39	3.290	0.28065	-0.3	3.38
E	0.008651 ± 0.000011	1.467464 ± 0.000031	0.001153 ± 0.000023	0.280742 ± 0.000010	-72.3 ± 0.35	3.290	0.28067	0.3	3.36
F	0.008640 ± 0.000010	1.467423 ± 0.000025	0.000695 ± 0.000022	0.280714 ± 0.000009	-73.2 ± 0.30	3.290	0.28067	0.4	3.35
G	0.008641 ± 0.000011	1.467460 ± 0.000027	0.000939 ± 0.000026	0.280710 ± 0.000009	-73.4 ± 0.31	3.290	0.28065	-0.3	3.38
H	0.008686 ± 0.000010	1.467441 ± 0.000029	0.001113 ± 0.000033	0.280758 ± 0.000009	-71.7 ± 0.32	3.290	0.28069	1.0	3.33
I	0.008652 ± 0.000011	1.467491 ± 0.000035	0.000787 ± 0.000011	0.280725 ± 0.000010	-72.8 ± 0.35	3.290	0.28068	0.6	3.35
J	0.008622 ± 0.000014	1.467454 ± 0.000040	0.001009 ± 0.000030	0.280719 ± 0.000011	-73.1 ± 0.40	3.290	0.28066	-0.1	3.37
312630 migmatite									
2.1	0.008635 ± 0.000012	1.467434 ± 0.000031	0.001315 ± 0.000020	0.280619 ± 0.000013	-76.6 ± 0.47	3.408	0.28053	-1.7	3.53
3.1	0.008662 ± 0.000013	1.467392 ± 0.000027	0.000744 ± 0.000005	0.280531 ± 0.000009	-79.7 ± 0.33	3.516	0.28048	-1.0	3.59
4.1	0.008672 ± 0.000014	1.467480 ± 0.000024	0.000816 ± 0.000008	0.280709 ± 0.000010	-73.4 ± 0.34	3.290	0.28066	-0.1	3.37
1.1	0.008678 ± 0.000013	1.467468 ± 0.000039	0.001189 ± 0.000026	0.280726 ± 0.000011	-72.8 ± 0.37	3.290	0.28065	-0.3	3.38
A*	0.008686 ± 0.000010	1.467454 ± 0.000026	0.001582 ± 0.000046	0.280647 ± 0.000011	-75.6 ± 0.40				3.52
B*	0.008665 ± 0.000017	1.467517 ± 0.000032	0.001380 ± 0.000021	0.280756 ± 0.000011	-71.7 ± 0.41				3.36
C*	0.008649 ± 0.000010	1.467389 ± 0.000028	0.000688 ± 0.000014	0.281002 ± 0.000014	-63.0 ± 0.51				2.98
D*	0.008647 ± 0.000009	1.467462 ± 0.000036	0.000967 ± 0.000024	0.280776 ± 0.000010	-71.0 ± 0.34				3.29

E*	0.008674 ± 0.000012	1.467466 ± 0.000028	0.001004 ± 0.000009	0.280663 ± 0.000010	-75.1 ± 0.36				3.44
F*	0.008672 ± 0.000019	1.467376 ± 0.000027	0.003116 ± 0.000034	0.280942 ± 0.000011	-65.2 ± 0.39				3.25
G*	0.008658 ± 0.000012	1.467479 ± 0.000033	0.001022 ± 0.000014	0.280659 ± 0.000012	-75.2 ± 0.44				3.45
H*	0.008655 ± 0.000016	1.467454 ± 0.000036	0.001954 ± 0.000013	0.280577 ± 0.000011	-78.1 ± 0.39				3.64
I*	0.008663 ± 0.000007	1.467475 ± 0.000021	0.000701 ± 0.000012	0.280899 ± 0.000008	-66.7 ± 0.27				3.12
J*	0.008640 ± 0.000014	1.467399 ± 0.000026	0.002751 ± 0.000043	0.280939 ± 0.000009	-65.3 ± 0.30				3.23
K*	0.008658 ± 0.000016	1.467435 ± 0.000025	0.003181 ± 0.000029	0.280680 ± 0.000012	-74.4 ± 0.43				3.62
L*	0.008708 ± 0.000020	1.467477 ± 0.000039	0.002478 ± 0.000057	0.280848 ± 0.000012	-68.5 ± 0.43				3.33
M*	0.008702 ± 0.000026	1.467434 ± 0.000027	0.002498 ± 0.000053	0.280975 ± 0.000013	-64.0 ± 0.48				3.16
N*	0.008652 ± 0.000016	1.467403 ± 0.000026	0.002111 ± 0.000031	0.280980 ± 0.000009	-63.8 ± 0.31				3.12
312631 metagranite									
1.1	0.008646 ± 0.000011	1.467420 ± 0.000026	0.000397 ± 0.000002	0.280689 ± 0.000009	-74.1 ± 0.33	3.290	0.28066	0.2	3.36
2.1	0.008682 ± 0.000016	1.467430 ± 0.000034	0.001163 ± 0.000052	0.280650 ± 0.000011	-75.5 ± 0.39	3.290	0.28058	-2.9	3.47
3.1	0.008658 ± 0.000008	1.467471 ± 0.000030	0.000459 ± 0.000021	0.280917 ± 0.000010	-66.0 ± 0.35	3.290	0.28089	8.2	3.07
4.1	0.008646 ± 0.000019	1.467544 ± 0.000040	0.001056 ± 0.000015	0.280776 ± 0.000013	-71.0 ± 0.45	3.290	0.28071	1.8	3.30
5.1	0.008663 ± 0.000017	1.467396 ± 0.000034	0.001278 ± 0.000038	0.280749 ± 0.000013	-72.0 ± 0.47	3.290	0.28067	0.3	3.36
6.1	0.008679 ± 0.000010	1.467383 ± 0.000041	0.000750 ± 0.000005	0.280640 ± 0.000012	-75.9 ± 0.42	3.290	0.28059	-2.4	3.45
7.1	0.008662 ± 0.000012	1.467446 ± 0.000031	0.000966 ± 0.000029	0.280613 ± 0.000011	-76.8 ± 0.39	3.290	0.28055	-3.8	3.51
A	0.008666 ± 0.000018	1.467510 ± 0.000030	0.001410 ± 0.000072	0.280748 ± 0.000012	-72.0 ± 0.41	3.290	0.28066	0.0	3.37
B	0.008634 ± 0.000010	1.467421 ± 0.000032	0.001062 ± 0.000010	0.280697 ± 0.000012	-73.8 ± 0.43	3.290	0.28063	-1.0	3.41
C	0.008671 ± 0.000012	1.467430 ± 0.000027	0.000820 ± 0.000016	0.280747 ± 0.000010	-72.1 ± 0.35	3.290	0.28069	1.3	3.32
D	0.008665 ± 0.000015	1.467424 ± 0.000036	0.001274 ± 0.000032	0.280739 ± 0.000014	-72.4 ± 0.49	3.290	0.28066	0.0	3.37
E	0.008656 ± 0.000010	1.467288 ± 0.000150	0.000826 ± 0.000017	0.280647 ± 0.000023	-75.6 ± 0.82	3.290	0.28059	-2.3	3.45
G	0.008664 ± 0.000018	1.467377 ± 0.000031	0.001125 ± 0.000061	0.280679 ± 0.000014	-74.5 ± 0.48	3.290	0.28061	-1.8	3.43
312696 metagranodiorite									
1.1	0.008656 ± 0.000011	1.46739 ± 0.000030	0.000402 ± 0.000008	0.280678 ± 0.000010	-74.5 ± 0.34	3.292	0.28065	-0.2	3.4
2.1	0.008654 ± 0.000015	1.46750 ± 0.000046	0.000899 ± 0.000017	0.280718 ± 0.000014	-73.1 ± 0.48	3.292	0.28066	0.1	3.4
3.1	0.008664 ± 0.000012	1.46742 ± 0.000032	0.000533 ± 0.000013	0.280688 ± 0.000013	-74.1 ± 0.45	3.292	0.28065	-0.1	3.4
4.1	0.008653 ± 0.000013	1.46753 ± 0.000041	0.000306 ± 0.000011	0.280666 ± 0.000015	-74.9 ± 0.53	3.292	0.28065	-0.4	3.4
5.1	0.008675 ± 0.000015	1.46734 ± 0.000040	0.000427 ± 0.000004	0.280669 ± 0.000013	-74.8 ± 0.46	3.292	0.28064	-0.5	3.4
6.1	0.008661 ± 0.000012	1.46732 ± 0.000051	0.000721 ± 0.000016	0.280695 ± 0.000015	-73.9 ± 0.52	3.292	0.28065	-0.3	3.4
7.1	0.008660 ± 0.000018	1.46742 ± 0.000043	0.000830 ± 0.000034	0.280716 ± 0.000014	-73.2 ± 0.48	3.292	0.28066	0.2	3.4
8.1	0.008664 ± 0.000011	1.46741 ± 0.000028	0.000416 ± 0.000010	0.280672 ± 0.000010	-74.7 ± 0.35	3.292	0.28065	-0.4	3.4
A	0.008666 ± 0.000012	1.46748 ± 0.000036	0.001395 ± 0.000022	0.280782 ± 0.000013	-70.8 ± 0.46	3.292	0.28069	1.3	3.3
B	0.008649 ± 0.000012	1.46742 ± 0.000030	0.001173 ± 0.000027	0.280740 ± 0.000009	-72.3 ± 0.33	3.292	0.28067	0.3	3.4
C	0.008668 ± 0.000013	1.46737 ± 0.000034	0.001088 ± 0.000008	0.280709 ± 0.000012	-73.4 ± 0.41	3.292	0.28064	-0.6	3.4
D	0.008637 ± 0.000010	1.46741 ± 0.000026	0.000506 ± 0.000018	0.280678 ± 0.000008	-74.5 ± 0.30	3.292	0.28065	-0.4	3.4
E	0.008640 ± 0.000012	1.46745 ± 0.000029	0.001116 ± 0.000010	0.280731 ± 0.000009	-72.6 ± 0.33	3.292	0.28066	0.1	3.4
F	0.008663 ± 0.000012	1.46746 ± 0.000028	0.000968 ± 0.000015	0.280721 ± 0.000010	-73.0 ± 0.34	3.292	0.28066	0.1	3.4

312653 paragneiss

3.1	0.008621 ± 0.000022	1.467385 ± 0.000032	0.001375 ± 0.000076	0.280964 ± 0.000012	-64.4 ± 0.42	2.724	0.28089	-5.0	3.1
5.1	0.008655 ± 0.000016	1.467350 ± 0.000036	0.000555 ± 0.000020	0.280808 ± 0.000013	-69.9 ± 0.46	2.711	0.28078	-9.4	3.2
5.1	0.008670 ± 0.000020	1.467413 ± 0.000064	0.000801 ± 0.000012	0.280906 ± 0.000029	-66.5 ± 1.04	2.711	0.28086	-6.3	3.1
7.1	0.008628 ± 0.000010	1.467452 ± 0.000026	0.000528 ± 0.000004	0.280818 ± 0.000010	-69.5 ± 0.36	2.714	0.28079	-8.9	3.2
8.1	0.008636 ± 0.000011	1.467395 ± 0.000031	0.000492 ± 0.000004	0.281022 ± 0.000012	-62.4 ± 0.42	2.917	0.28099	3.1	2.9
9.1	0.008645 ± 0.000016	1.467434 ± 0.000029	0.001548 ± 0.000036	0.281113 ± 0.000013	-59.1 ± 0.47	2.836	0.28103	2.5	2.9
10.1	0.008657 ± 0.000011	1.467383 ± 0.000025	0.000699 ± 0.000005	0.281022 ± 0.000011	-62.4 ± 0.39	2.707	0.28099	-2.1	3.0
11.1	0.008651 ± 0.000008	1.467465 ± 0.000027	0.000248 ± 0.000007	0.280928 ± 0.000009	-65.7 ± 0.32	2.963	0.28091	1.4	3.0
12.1	0.008634 ± 0.000015	1.467505 ± 0.000037	0.000740 ± 0.000010	0.280961 ± 0.000013	-64.5 ± 0.47	2.728	0.28092	-3.9	3.0
13.1	0.008649 ± 0.000017	1.467412 ± 0.000034	0.000977 ± 0.000028	0.281060 ± 0.000011	-61.0 ± 0.39	2.708	0.28101	-1.3	2.9
18.1	0.008632 ± 0.000013	1.467449 ± 0.000039	0.000709 ± 0.000009	0.281028 ± 0.000010	-62.1 ± 0.35	2.928	0.28099	3.2	2.9
A*	0.008660 ± 0.000011	1.467399 ± 0.000029	0.000870 ± 0.000030	0.281012 ± 0.000010	-62.7 ± 0.36				3.0
A*	0.008660 ± 0.000011	1.467399 ± 0.000029	0.000870 ± 0.000030	0.281012 ± 0.000010	-62.7 ± 0.36				3.0
B*	0.008648 ± 0.000005	1.467331 ± 0.000043	0.000202 ± 0.000009	0.280934 ± 0.000010	-65.5 ± 0.36				3.0
C*	0.008662 ± 0.000012	1.467391 ± 0.000031	0.000496 ± 0.000006	0.281029 ± 0.000011	-62.1 ± 0.41				2.9
D*	0.008650 ± 0.000011	1.467419 ± 0.000030	0.000475 ± 0.000016	0.280889 ± 0.000012	-67.1 ± 0.41				3.1
E*	0.008649 ± 0.000011	1.467423 ± 0.000027	0.000625 ± 0.000004	0.281034 ± 0.000010	-61.9 ± 0.35				2.9
F*	0.008644 ± 0.000009	1.467494 ± 0.000037	0.001030 ± 0.000025	0.280722 ± 0.000010	-73.0 ± 0.36				3.37

312658 paragneiss

3.1	0.008663 ± 0.000012	1.467405 ± 0.000032	0.000874 ± 0.000011	0.280998 ± 0.000012	-63.2 ± 0.42	2.706	0.28095	-3.3	3.0
4.1	0.008652 ± 0.000012	1.467386 ± 0.000032	0.000582 ± 0.000014	0.281104 ± 0.000010	-59.4 ± 0.37	2.711	0.28107	1.1	2.8
5.1	0.008655 ± 0.000013	1.467413 ± 0.000029	0.000633 ± 0.000012	0.281050 ± 0.000011	-61.4 ± 0.39	2.708	0.28102	-1.0	2.9
7.1	0.008662 ± 0.000012	1.467418 ± 0.000031	0.000722 ± 0.000017	0.281095 ± 0.000011	-59.8 ± 0.39	2.704	0.28106	0.4	2.9
8.1	0.008673 ± 0.000014	1.467361 ± 0.000035	0.000695 ± 0.000021	0.280969 ± 0.000014	-64.2 ± 0.49	2.735	0.28093	-3.4	3.0
9.1	0.008647 ± 0.000011	1.467374 ± 0.000027	0.000659 ± 0.000003	0.280957 ± 0.000013	-64.7 ± 0.45	2.731	0.28092	-3.8	3.0
10.1	0.008652 ± 0.000012	1.467407 ± 0.000033	0.000556 ± 0.000013	0.280906 ± 0.000010	-66.4 ± 0.37	2.721	0.28088	-5.7	3.1
14.1	0.008652 ± 0.000010	1.467459 ± 0.000030	0.000384 ± 0.000006	0.281012 ± 0.000011	-62.7 ± 0.38	2.916	0.28099	3.0	2.9
15.1	0.008675 ± 0.000015	1.467473 ± 0.000031	0.000607 ± 0.000008	0.281023 ± 0.000011	-62.3 ± 0.38	2.715	0.28099	-1.7	2.9
18.1	0.008654 ± 0.000009	1.467385 ± 0.000030	0.000317 ± 0.000006	0.281022 ± 0.000011	-62.3 ± 0.38	2.892	0.28100	2.9	2.9
19.1	0.008693 ± 0.000011	1.467447 ± 0.000031	0.001030 ± 0.000020	0.281147 ± 0.000012	-57.9 ± 0.42	2.858	0.28109	5.2	2.8
A*	0.008653 ± 0.000053	1.467447 ± 0.000039	0.001549 ± 0.000110	0.281110 ± 0.000021	-59.2 ± 0.75				2.9
B*	0.008656 ± 0.000012	1.467406 ± 0.000025	0.000669 ± 0.000018	0.281016 ± 0.000013	-62.6 ± 0.47				3.0
C*	0.008660 ± 0.000048	1.467297 ± 0.000052	0.001173 ± 0.000076	0.281032 ± 0.000017	-62.0 ± 0.62				3.0

CHUR values from Bouvier et al, 2008.

1. This uncertainty is the in-run standard error.
2. Depleted mantle model ages calculated using $^{176}Hf/^{177}Hf = 0.282785$ for the modern upper mantle and $^{176}Lu/^{177}Hf=0.0336$.

* data in paragneisses and migmatites where there is no U-Pb age data for the site. Only DM, not initial, ages calculated.

Table 4. Age contrasts between the 'polar' and 'southern' continents

	2.5-3.23 Ga	3.26-3.5Ga	>3.6 Ga
southern continent	yes	no	yes
polar continent	yes	yes	no